8-2022

Curvilinear fractures in burned remains: an assessment of the relationship between fracture convexity and fire directionality

Kimber G. Cheek
University of Tennessee, Knoxville, kcheek3@utk.edu

To the Graduate Council:

I am submitting herewith a thesis written by Kimber G. Cheek entitled "Curvilinear fractures in burned remains: an assessment of the relationship between fracture convexity and fire directionality." I have examined the final electronic copy of this thesis for form and content and recommend that it be accepted in partial fulfillment of the requirements for the degree of Master of Arts, with a major in Anthropology.

Lee M. Jantz, Major Professor

We have read this thesis and recommend its acceptance:

Dawnie W. Steadman, Joanne L. Devlin

Accepted for the Council:
Dixie L. Thompson

Vice Provost and Dean of the Graduate School

(Original signatures are on file with official student records.)

Curvilinear fractures in burned remains: An assessment of the relationship between fracture convexity and fire directionality

A Thesis Presented for the
Master of Arts
Degree
The University of Tennessee, Knoxville

Kimber Grace Cheek
August 2022

ACKNOWLEDGEMENTS

Thank you to the IACUC office, the JRTU staff, the LAC students and faculty, Dr. Strickland, and the O'Rourke family in their assistance on the procurement of my sample, to the FAC students and staff who helped with the disarticulation of my sheep and/or the burn days Liz Ronald, Kelley Cross, Karli Palmer, Kathleen Hauther, Marta Paulson, Stephanie House, Matt Davis, Mary Davis, and many more, to Dr. Mundorff for the use of her FLIR, to Dr. Janzen and Jen Green for their assistance in the freezing of the sheep, to the staff from the University of Tennessee's Forest Resources Agresearch and Education Center, to my committee members Drs. Meadows Jantz, Steadman, and Devlin, to Tati and Fred for keeping me sane, to my friends and family for supporting me no matter what, without everyone above this project could not have happened.

ABSTRACT

Burned remains present a challenge for forensic anthropologists due to the variable nature of fires, the unique way fires impact remains, and the impact of heat changes on the analysis of the remains. A topic of extensive study is the fracture patterns seen in burned remains. Curvilinear fractures are one type of fracture that was originally discussed in the context of studying the preburned state of remains (Baby, 1954; Binford, 1963; Buikstra and Swegle, 1989). These fractures are thought to be created through the kinetic energy generated as muscles shrink and pull on the periosteum, fracturing the bone below (Symes et al., 2008). The convexity of the curvilinear fracture has been theorized to indicate the direction heat moved along bone and, more specifically, points towards the direction of the heat source (Pope, 2007; Symes et al., 2008). To assess the relationship between fracture convexity and fire directionality, the limbs of four sheep were burned in pairs with the dorsal side down and the caudal end away from the origin of the fire. During the burns, video footage was recorded, and observation notes were taken. Qualitative observations were summarized using the burn notes, videos, and recovered bones. These observations documented the pattern of limb destruction and movement, color and uniformity of the burn pattern per bone, and all instances of curvilinear fractures and the direction of these fractures. A total of 18 curvilinear fractures were seen on 17 of the 56 bones examined. Of these 18 fractures, 14 were convex distally which was the predicted direction and four were convex proximally. An *a posteriori* power analysis was conducted and found that a sample size of 32 would be needed for a repetition of this study to have high power and effect size. In this preliminary study, conclusions suggest that curvilinear fractures are not related to fire directionality but likely indicate how heat moves along a bone. With a larger sample size, there are many avenues to further assess how curvilinear fractures are created and what information they can contribute to the anthropological analysis of burned remains.

TABLE OF CONTENTS

LIST OF TABLES

LIST OF FIGURES

CHAPTER ONE

INTRODUCTION

Forensic anthropologists are called upon to apply their knowledge of the human skeletal system to cases that involve remains that are either no longer identifiable or in cases where specialized knowledge of human osteology is needed. They assist in determining if the remains are human or nonhuman, creating a biological profile, conducting trauma analysis, and completing an analysis of the taphonomic processes that altered the remains after death, including burning. Fire cases pose a unique challenge for both anthropologists and the law enforcement officials with whom they work. Fire is a common mechanism for evidence destruction, but destroying human remains completely is not easy to accomplish (Warren and Shultz, 2002; Symes et al., 2014). When human remains are burnt, they become fragile and highly fragmented, making analysis difficult. A common misconception is when remains are burned they will be the consistency of commercial cremains. Fire can extensively damage bone causing changes in color, fracturing, and deformation; but even a high temperature fire that burns for a long duration can leave behind identifiable pieces of bone (Symes et al., 2008; Pope and Smith, 2004). Even if burned fragments are unknown in origin, histology can help identify if the fragment is bone and if the bone belongs to a human or an animal (Hillier and Bell, 2007). DNA can sometimes be used for more detailed information on the biological profile of the individual (Latham and Madonna, 2014). Burning remains to attempt to disguise perimortem trauma is a heavily studied topic in forensic anthropology. Pope and Smith (2004) found that it is possible to distinguish cranial fractures created by trauma from those formed during burning. Research has found that sharp force and blunt force trauma cab be identifiable despite the remains being burned (Herrmann and Bennett, 1999; Macoveciuc et al., 2017; Marciniak, 2009; Pope and Smith, 2004).

The extent of thermal damage to human remains is variable based on the dynamics of the fire; its size, burn time, temperature, environment, the body's proximity to the fire, and fuel type all influence how the remains will be altered (Symes et al., 2008). Due to this variability, a vast amount of literature has been written regarding different aspects of how fire affects human remains. Much of the early literature is based on the archaeological investigation of cremains but has since expanded to focus on experiments to broaden the understanding of how fire impacts remains. These experiments are designed to test how fire size, burn time, temperature, environment, the body's proximity to the fire, and fuel type specifically impact remains and how the burning of remains influences the anthropological analysis (Thompson, 2005; Baby, 1954; Binford, 1963; Buikstra and Swegle, 1989). Experiments range from how temperature affects the color and fracture patterns of burned bone (Shipman at al., 1984; Buikstra and Swegle, 1989), to studies looking at the effect of burning on the estimation of the biological profile (Thompson, 2005; Eckert et al., 1998), to studies identifying the best way to preserve the bones postburn (Siegert et al., 2018; Rossi et al., 2004; Topoleski and Christensen, 2019). While many questions about how fire affects remains have been answered, there is still an ever-growing list of unanswered questions.

One of the earliest questions asked by archaeologists was what features of burned bone can be used to identify the preburned state of the body (Baby, 1954; Binford, 1963; Buikstra and Swegle, 1989). A key feature that is assumed to only occur in remains that are fleshed (or "green"), is known as a curvilinear fracture, also known as curved transverse, thumbnail, or tissue regression fractures (Buiksta and Swegle, 1989; Pope, 2007; Symes et al., 2008). These fractures are commonly thought to be created through the kinetic energy generated by muscle fibers as they shrink away from a fire (Pope, 2007; Symes et al., 2008; Williams, 2020).

In the book, *The Analysis of Burned Human Remains*, Symes and colleagues (2008) include in a caption that curvilinear fractures are concave in the direction of the retreating tissue. If the muscle fibers are shrinking away from the heat source, the body's position

relative to heat could potentially be inferred based on the direction of the fractures. Pope (2007) discusses how the convexity of a curvilinear fracture points in the direction of the heat source. Curvilinear fractures and their relationship to muscle fibers have been mentioned in several studies, but there are no studies assessing the relationship between the convexity or concavity and the body's position related to the fire (Pope, 2007; Symes et al., 2008). This thesis is a preliminary experiment to assess the relationship between fracture convexity, fire directionality, and tissue shrinkage. Fracture pattern analysis is an important tool for anthropologists interpreting burned remains and the dearth of information surrounding curvilinear fractures makes their use in the analysis of burned remains imprecise. The hypothesis is that there is a relationship between the convexity of a curvilinear fracture and the body's position relative to a fire. For this thesis the sample will be placed with the origin of the fire at their caudal end. If curvilinear fracture convexity is related to body position relative to the fire, then all of the curvilinear fractures present in the sample will be convex distally.

CHAPTER TWO
LITERATURE REVIEW

Burned Remains and Anthropology

The study of burned remains in anthropology originated in the study of cremains found in archaeological contexts and has since expanded to applications in forensic anthropology. The beginning of the field of anthropology's interest in cremations and the patterns of thermal damage to bones sprouted from the curiosity of archaeologists about what information these patterns could provide about when, how, and why the remains were burned (Baby, 1954; Binford, 1963; Buikstra and Swegle, 1989). The main questions they asked were how does burning influence anthropological interpretation, was the burning intentional, if so, how did the cremation play into the funerary rites of the people, and what can be said about the state of the pre-burned condition of the body (Binford, 1963; Buikstra and Swegle, 1989). The burning of remains inherently alters bone, but there is little understanding to what extent these changes impact anthropological methods traditionally used in the interpretation of a site. Many studies sought to categorize how shrinkage and warping impact methods associated with the biological profile (Mamede et al., 2018; Thompson, 2004, 2005; Ubelaker, 2009). Varying levels of thermal alteration can impact morphological and metric methods of biological profile estimation (Mamede et al., 2018; Thompson, 2004, 2005; Ubelaker, 2009). Others sought to classify the difference between fractures created by burning and the traumatic injuries to bone occurring prior to burning (Herrmann and Bennett, 1999; Macoveciuc et al., 2017; Marciniak, 2009; Pope and Smith, 2004). Sharp force trauma is easily distinguished from thermal trauma, while blunt force trauma is more complicated to distinguish (Herrmann and Bennett, 1999; Macoveciuc et al., 2017). Methods of interpretation such as ash weight and studies to classify the heat and duration of the fire used to burn the remains were created (Bohnert et al., 1998; Buikstra and Swegle, 1989; Goncalves et al., 2013; Trotter and Peterson, 1955). Many sought to classify how and when broad pattens of thermal damage, including color changes, fractures, and dimensional changes, occurred

(Borrini et al., 2012; Carrol and Smith, 2018; Pope, 2007; Reidsma et al., 2016; Williams, 2020).

One question that was thought to be the key to interpreting cremains in an archaeological context was if the preburned state of the remains can be interpreted (Buikstra and Swegle, 1989; Goncalves et al, 2015). Krogman was one of the first to explore the possibility of estimating whether the remains were fleshed, defleshed, or dry at the time of burning through his analysis of the Adena and Hopewell cremations for Webb and Snow (Webb and Snow, 1945). Webb and Snow invited Krogman to aid in analyzing these cremations based on his discussion of forensic fire investigations in the FBI Law Enforcement Bulletin (Krogman, 1943). According to Krogman (1943) it was fairly simple to tell the two apart. A dry bone exhibits cracks in a step-like, patina check pattern, and fleshed bone would only be partially incinerated and not show the checkered pattern of cracks (Krogman, 1943; Webb and Snow, 1945). He concluded that the remains at Hopewell had been cremated after the remains were skeletonized. But, as subsequent studies would show, the interpretation of the preburned state of remains is not as simple as Krogman suggested.

Following Krogman's assessment, Baby (1954), followed closely by Binford (1963), conducted experiments to test Krogman's thoughts, then applied findings to their own interpretations of cremations at archaeological sites. Baby disagreed with Krogman on his interpretation that a checking pattern and complete calcination can only be found on bone burned in a dry state. He argued that the cremations at the Hopewell site were fleshed and not dry (Baby, 1954). Baby tested his theory by burning a whole cadaver and what he called "'green bones' from the dissection room" and concluded that many of the features described by Krogman as being characteristic of bones burned dry are seen on the bones burned in the flesh from his test (Baby, 1954 p.4). Alternatively, Binford (1963) also experimented to build on what Baby found and agreed with Krogman that the bone burned in the flesh or green could be easily distinguished from those burned when dry. Binford (1963) used a combination of archaeological remains, macerated anatomical

specimens, and a green monkey cadaver as his sample that were burned over a charcoal fire. The green monkey was used as the green and fleshed bone sample, and Binford (1963) described the thermal fracture pattern to consist of deep, transverse fractures that are often curved and show the presence of warping. Binford noted that the degree of burning in fleshed remains could be attributed to factors including the amount of protective tissue, time burned, fire temperature, and position of the bone relative to the fire origin. Binford (1963) applied his finding to three Michigan archaeological sites where cremated remains were found. He concluded that, like the Hopewell cremations, the state of the cremations at the Michigan sites also suggested that the remains were burned in the flesh (Binford, 1963).

The experiments conducted by both Baby (1954) and Binford (1963) provided a good starting point for experimental work seeking to classify the traits of whether remains were burned in the flesh, but both lacked consistency and detailed results. Buikstra and Goldstein (1973) noted this lack of distinction and the potential for large variations to be seen in the study of remains burned in the flesh. Thurman and Willmore (1980) replicated the work done by Baby (1954) and Binford (1963) to try and clearly define the terms and patterns seen in previous articles, focusing on whether or not there was a difference between the burn patterns of fleshed and green bone. They found that bone burned while fleshed exhibited deep, transverse fractures, sometimes curved, and defleshed green bone only exhibited the checking pattern described by Binford (1963) and Baby (1954) (Thurman and Wilmore, 1980). Thurman and Wilmore (1980) hypothesized that had they allowed the fleshed samples to continue to burn to the point of calcination, they too would show the checked pattern along with deep, transverse fractures.

Buikstra and Swegle (1989) decided that a more detailed laboratory study should be conducted using remains that were not chemically treated, like the bones of laboratory specimens used by Binford (1963), Baby (1954), and Thurman and Wilmore (1980). Using unaltered fleshed, green, and dry human, pig, and dog bones, they thoroughly documented the thermal damage seen on bones both smoked (charred) and calcined

(Buikstra and Swegle, 1989). Their findings differed from previous studies in several ways. They found that no matter the preburned state of the remains, longitudinal splitting was present, though in dry bone, they were often shallower and less frequently accompanied by transverse cracking seen in their fleshed and green samples (Buikstra and Swegle, 1989). The curved transverse fractures Thurman and Wilmore (1980) characterized as a key feature of bones burned in the flesh was also observed in Buikstra and Swegle's (1989) green defleshed sample. The importance of bone color as an indicator of a preburned state was highlighted as a more distinct tool than fracture pattern analysis (Buikstra and Swegle, 1989). Buikstra and Swegle (1989) argued that the color distinction between burned fleshed or green and dry bones was a much clearer indicator than the fracture pattern. They, like Krogman (1943), note that the presence of unburned portions of bone are the best indicator of bones burned in the flesh (Buikstra and Swegle, 1989). Ultimately, they concluded that while the pattern between thermal alterations and the preburned state of the remains was not as straightforward as previously stated, with more research, a distinction between the thermal damage could be observed and correlated to the preburned condition of the remains (Buikstra and Swegle, 1989). A recent study by Lemmers and colleagues (2020) found that the preburned condition of remains can be assessed through a histological examination of bioerosion. Bioerosion is the degradation of bone tissues organic and inorganic components and histological signs of bioerosion can be examined to predict how long the remains were allowed to decompose naturally compared to a sped-up form of flesh removal (Lemmers et al., 2020). Signs of bioerosion are seen histologically as the degradation of feature of the haversian system, including lacunae and canaliculi, as well as splitting of the haversian systems and carbon inclusions which appear as dark smudges in the bone tissue (Lemmers et al., 2020). Lemmers and colleagues (2020) found that these signs of bioerosion persisted post burning, allowing for an assessment of the amount of decomposition that occurred before the remains were burned and thus what state the remains were in prior to burning.

Other than studies that focus on the broad patterns of thermal damage, more specific studies focus on different thermal damage elements and seek to understand their cause or how they are interpreted. Some examples include how the color change that occurs during burning are tied to the duration and temperature of the fire (Bonucci and Graziani, 1975; McCutcheon, 1992; Shipman et al., 1984), how burning affects trauma analysis (Herrmann and Bennett, 1999; Marcniak, 2019), how burning affects the interpretation of histology (Fernandez Castillo et al., 2006; Lemmers et al., 2020), how chronological age affects thermal damage (Waterhouse, 2013; Zana et al., 2017), and what information can be gleaned from cremation weights (Goncalves et al., 2013; Trotter and Peterson, 1955). Like the disagreement between Krogman and Baby about the preburned state of the Hopewell cremations, there is much disagreement in studies that test the same feature of how burning affects human remains. An example is the temperature gradients that correspond to color change. There is consensus that temperature and exposure are directly linked with color change in burned bone, but the ranges of temperature and color change created based on observations during experimentation vary (Bonucci and Graziani, 1975; McCutcheon, 1992; Shipman et al., 1984). These disagreements are rooted in a large number of variables in experiments involving the burning of remains. Fire is fed by fuel and oxygen. The temperature and duration of a fire are influenced by the environment, the fuel type used, and the remains being burned. Some experiments were conducted within cremation chambers with controlled temperature and times (Ellingham and Sandholzer, 2020; Reidsma et al., 2016; Thompson and Chudek, 2007). These experiments allow for a better understanding of the exact temperatures at which thermal changes occur, but the overly controlled environment does not mimic what would happen on a wooden pyre or in a house fire. Field experiments in different contexts with different fuel types are harder to control and produce variable data but shed more light on what would be observed at an archaeological site or a forensic fire scene (Carrol and Smith, 2018). As a result, many studies involving fire's effects on bone have shifted to focus on sweeping generalities or very specific questions. One example of both is fracture pattern analysis.

Fracture Formation

Before discussing fracture pattern analysis, it is important to know the basic biomechanics of fractures and the specifics of fractures in burned remains. There are physiological and molecular influences on how a bone fractures including bone size, shape, bone porosity, bone cortical thickness, and mineral and collagen content (Davidson et al., 2006). A bone's ability to react to stress and strain is influenced by changes or differences in the physiological and molecular properties (Davidson et al., 2006). In burned remains, bone collagen content is thought to be a major factor influencing the formation of thermal fractures (Davidson et al., 2006; Agnew and Bolte, 2012; Bertocci et al., 2017; Goncalves et al., 2011).

Collagen content in bone acts to both increase strength and to absorb energy (Davidson et al., 2006; Agnew and Bolte, 2012). A higher amount of energy is needed to fracture bones with high collagen content than to fracture bones that have high mineralization (Bertocci et al., 2017). As a bone burns it dehydrates and the collagen cells contract (Goncalves et al., 2011). The dehydration of the bone causes it to become more brittle and as the collagen cells contract, they generate force (Goncalves et al., 2011; Symes et al., 2008; Symes et al, 2014). The force generated by the contracting collagen is thought to be able to act on the mineral portion of bone (Goncalves et al., 2011). As the bone dehydrates, shrinks, and the collagen contracts, it can cause the bone to fail (Goncalves et al., 2011; Symes et al., 2014). As well as the intrinsic factors of bone that influence fracturing in burned remains, extrinsic factors may also impact the formation of fractures.

Extrinsic factors can include preexisting trauma or conditions influencing bone quality and forces from the burn environment (Agnew and Bolte, 2012). One of these extrinsic factors will only impact remains burned in the flesh and it is the kinetic energy generated by muscle fibers contraction as they burn. The retreating muscle fibers pull on the periosteum, which fractures the brittle bone underneath (Symes et al., 2008). There is a lack of agreement in the study of burned remains as to whether or not the kinetic energy

generated by shrinking muscle tissue has enough force to influence the creation of fractures (Thompson, 2005). The intrinsic factors are more likely to influence the formation of fractures in burned remains.

Fracture Pattern Analysis and Curvilinear Fractures

There are several different types of heat-related fractures, delamination, longitudinal, transverse, and curvilinear. Delamination fractures, which occur in burned crania, are expressed as a separation of the external table from the diploe (Pope, 2007; Symes et al., 2008; Williams, 2020). Longitudinal fractures are seen as long deep splits along the axis of a bone, while transverse fractures are splits against the grain of the bone (Pope, 2007; Symes et al., 2008; Williams, 2020). These three fractures occur primarily along the shafts of long bones, but they can also be seen less frequently on other types of bones (Pope, 2007; Symes et al., 2008; Williams, 2020). These three fractures are seen in remains burned in the flesh, green, and dry bone as they are a direct result of the dimensional changes that occur due to shrinkage (Pope, 2007; Symes et al., 2008; Williams, 2020). Shrinkage occurs first in the external cortex of bone and proceeds deeper the longer the bone is exposed to heat (Ellingham et al., 2015; Ellingham and Sandholzer, 2020). The last type of thermal fracture is the curvilinear fracture. Curvilinear fractures are seen as a series of transversely oriented curved fractures commonly along the shaft of long bones and on joint surfaces (Symes et al., 2008).

Many scientists have attempted to research the causes of curvilinear fractures but there is no consensus. One theoretical mechanism for creating curvilinear fractures is through the kinetic energy generated as the muscle fibers dehydrate and contract along the long axis of the bone away from the heat source (Pope, 2007; Symes et al., 2008; Thompson, 2005). When discussing how bone warps when burned, Thompson (2005) claims that the theory that these fractures and warping are caused by the kinetic energy building up in contracting muscle is “speculative and not substantiated by quantitative data”,

particularly when warping is also present in bone burned without the presence of flesh (Thompson, 2005).

Goncalves and colleagues (2011) suggest that curvilinear fractures and warping may occur due to collagen content of the bone at the time of burning. To test this, they burned 96 fleshed human cadavers and 85 dry human skeletons and recorded the prevalence of curvilinear fractures (Goncalves et al., 2011). Similar to previous studies (Baby, 1954; Binford, 1963; Buikstra and Swegle, 1989; Thurman and Wilmore, 1980), Goncalves and colleagues (2011) found that the curvilinear fractures occurred more commonly in the fleshed or green remains but, unlike those before, found that curvilinear fractures can also occur in dry remains, though rarely. They suggest that warping and curvilinear fractures may be a better indicator of bone collagen content at the time of burning rather than the presence of flesh on the remains (Goncalves et al., 2011). Vassalo and colleagues (2016) found that while collagen content does play a significant role in the warping of burned bone, it has less of an effect on bone warping than burn time and temperature. Despite the varying opinions in the field on the factors influencing the creation of curvilinear fractures and whether or not they only occur in fleshed remains, several authors have referenced a relationship between curvilinear fractures and the regression of flesh (Pope, 2007; Symes et al., 2008; Williams, 2020).

Symes and colleagues (2008) suggest that the direction of curvilinear fractures is related to how heat moves along the bone. Pope (2007) calls these fractures curved tissue regression fractures, describing the process of the muscle shrinking away from the fire, pulling on the periosteum, and creating the fractures in the brittle underlying bone in the direction the fire consumed the bone. Pope (2007) cites Buikstra and Swegle (1989) in several instances when referring to the relationship between muscle, curvilinear fractures, and how the fractures map the progression of fire along a bone. Pope (2007) discusses how typically a body burns in a predictable pattern called the pugilistic pose. The pugilistic pose results from a series of well-documented changes a body goes through as it burns (Pope, 2007). Both limbs extend first and then curl inward as the flexor muscles

contract. The arms take on what is sometimes referred to as the boxer's pose in front of the torso with the hands curled into fists, and the knees pull up towards the torso with the feet flexing towards the shins (Pope, 2007; Symes et al., 2008; Williams, 2020). Pope (2007) suggests that if there is trauma to the body, whether dismemberment or extensive tissue trauma, it will create an abnormal burn pattern, and curvilinear fractures will be seen in the opposite direction than predicted.

One of the major issues with the relationship between curvilinear fractures and muscle contraction under heating is the lack of data to support this relationship. Many articles that note this relationship cite either Buikstra and Swegle (1989), Baby (1954), or Binford (1963), but none of these authors mention more than curvilinear fractures only occurring in fleshed or green remains (Goncalves et al., 2011, 2015, Pope, 2007; Symes et al., 2008, Thurman and Wilmore, 1980; Vassalo et al., 2016; Williams, 2020). Other articles anecdotally reference the relationship (Herrmann and Bennett, 1999; Macoveciuc et al., 2017). Symes and colleagues (2008) detail the process of the muscle fibers shrinking and creating kinetic energy that then fractures the bone. It is suggested that curvilinear fractures are convex in the direction of the heat source (Pope, 2007; Symes et al., 2008) (Figure 2.1). However, no source data exists to support these statements, nor were any experiments conducted to verify the claim. The relationship between curvilinear fractures, kinetic energy generated by muscle shrinkage, and the position of the body relative to the fire has not been validated.

Figure 2.1. Example of curvilinear fractures along the shaft of a tibia. The red arrow shows how the fire moved along the shaft of the bone and the direction in which the muscle receded. The blue arrows indicate the first curvilinear fracture.

CHAPTER THREE
MATERIALS AND METHODS

Materials

Nonhuman Model

Due to the destructive nature of this project, sheep (*Ovis aries*) were used as a nonhuman model. Many studies, including other burn studies, use sheep in place of pigs because they more closely simulate the average human due to their decreased muscle to fat ratio and their mix of haversian and plexiform bone cells (Thompson et al., 2011; Thompson and Chudek, 2007; Shipman et al., 1984; Macoveciuc et al., 2017; Dempsey et al., 2018; Thompson, 2005; Carroll and Smith, 2018). Four sheep were acquired from a local farmer as the sample for this study. Each limb was considered separate specimens, creating a sample size of 16 limbs. After going through the Institutional Animal Care and Use Committee (IACUC) process, the project was approved, and procedures were put in place to ensure the humane treatment of the animals. The sheep were purchased from a local farmer and humanely euthanized through anesthetic barbiturate overdose by a veterinarian from the Animal Sciences Department at the University of Tennessee, Knoxville. The sample consists of two juvenile male sheep 10 months old and 11 months old, a two-year-old male, and three-year-old female. The varying ages of the specimens bring about intrinsic differences in the bones of the sheep. The 10 and 11-month-old specimens will have a distinct lack of fusion in the epiphyses of the long bones, while the two- and three-year-old specimens will be fully fused. This difference may have impacted the creation of fractures around the ends of the long bones.

After euthanasia, the sheep were disarticulated, according to May (1970), to ensure the origins of all the muscles that insert on the limbs remain intact (Figure 3.1). For the hindlimb this involved cutting through the spine at or above T10, as the gluteal muscles that insert on the femur do not originate above T12 (Figure 3.1). For the forelimb all of the muscles that insert on the humerus originate on the scapula, so all of the muscles that insert on the scapula were severed to remove the limb (Figure 3.1). The

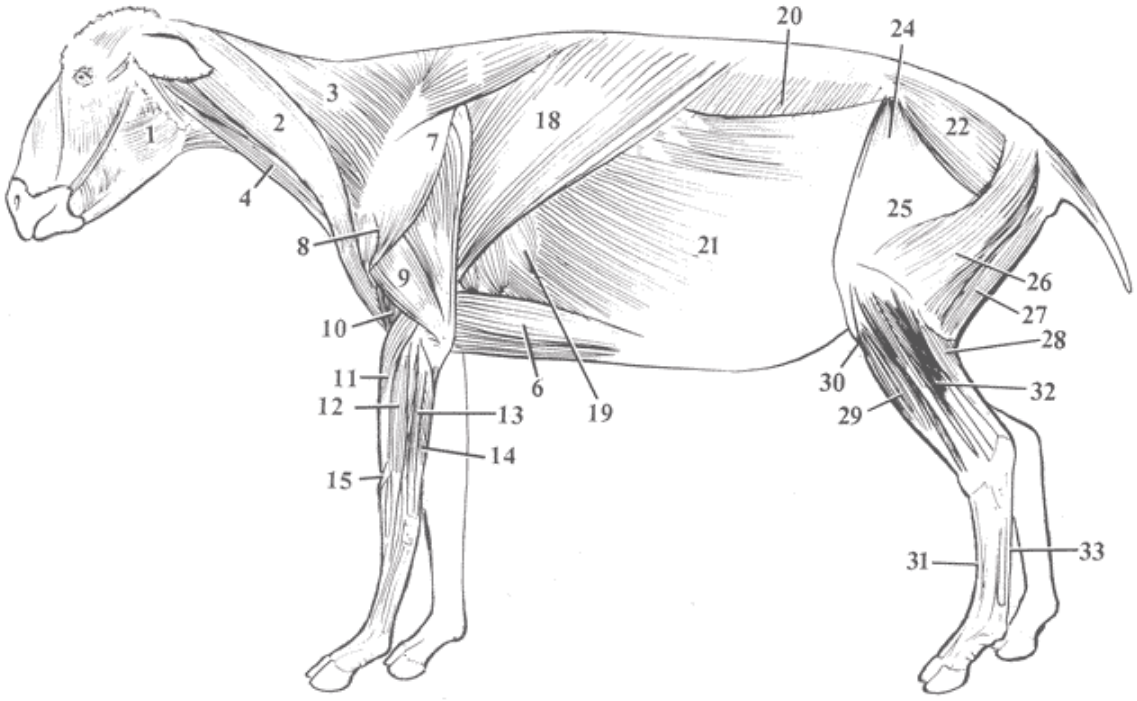

Figure 3.1. Sheep muscle anatomy diagram. 2. Brachiocephalicus 3. Trapezius 4. Sternocephalicus 6. Deep pectoral 7. Infraspinatus 8. Deltoid 9. Triceps brachii 10. Brachialis 11. Extensor carpi radialis 12. Extensor digitorum comminus 13. Extensor digitorum lateralis 14. Lateral ulnar 15. Oblique carpal extensor 17. Flexor carpi ulnaris (not shown) 22. Middle gluteal 24. Tensor fasciae latae 25. Vastus lateralis 26. Biceps femoris 27. Semitendinosus 28. Gastrocnemius 29. Third fibular 30. Tibialis cranialis 31. Long digital extensor 32. Deep digital flexor 33. Superficial digital flexor (Pasquini, et al., 1995).

disarticulation of the sheep allowed for easier handling and transportation of the specimens, for uniform placement of the specimens on the burn platform, and minimizes the time needed for decomposition after the burn. The weights of each pair of limbs can be found in Table 3.1. The remaining parts were donated to the Anthropology Department's Zooarchaeological teaching collection. After the disarticulation was completed, the remains were placed in freezers until roughly 10 days prior to their burning. The freezing of the remains can result in damage to the muscle tissues especially when multiple freeze and thaw cycles occur (Klop et al., 2017; Jung et al., 2011; Clavert et al., 2001; Pokines et al., 2016; Ren et al., 2012). Since freezing the sample was required for the timeline of this project, a single freeze/thaw cycle occurred, which is recommended for minimal damage to the muscle cells (Klop et al., 2017).

Burn Materials and Supplies

The burns were conducted on the University of Tennessee's Forest Resources Agresearch and Education Center property in Morgan County, Tennessee. The structure where the burns occurred was 4x6ft and made up of cinderblocks, rebar, metal chain link fence panel, and a sheet of small metal mesh (Figure 3.2). The structure was built with an opening on one side that goes to the ground. The opening acted as a port for putting fuel into the structure, lighting the fire, and allowing oxygen flow. Two Sony Fs5 cameras, lenses, and tripods were rented to record each burn. The camera choice was based on the recommendation of the Office of Student Media at the University of Tennessee, Knoxville. One camera was positioned on the side of the pyre with the opening, and another was placed to the left at the head of the pyre to record the changes to the remains as they burned. Acryloid™ B-72 was used as a consolidant to preserve the fragile bone post-burn and decomposition. Of the commercial consolidants and gelatin tested for the preservation of burned bone, Acryloid™ B-72 is the least destructive to bone, has the fastest dry time, and is not as messy as gelatin (Siegert et al., 2018; Rossi et al., 2004).

Table 3.1. Sheep and burn data.

Number	Age	Sex	Pair of Limbs	Weight (lbs)	Daily temp on burn day (F)	Duration of burn
2020-1	3yo	F	Forelimb	16	34-37	80min
			Hindlimb	30	52-63	300min
2020-2	2yo	M	Forelimb	38	35-40	80min
			Hindlimb	72	22-36	160min
2020-3	11mo	M	Forelimb	26	30-36	160min
			Hindlimb	53	32-49	180min
2020-4	10mo	M	Forelimb	22	32-40	120min
			Hindlimb	38	33-37	200min

Figure 3.2. 2020-1 Hindlimbs positioned on the burn structure with the dorsal side down and the caudal end positioned away from the origin of the fire.

Methods

Once the sheep limbs were allowed to defrost for 10 days, they were transported to the burn site and burned in limb pairs. The amount and type of wood used for fuel was fairly consistent between each trial but varied slightly due to the availability of wood. The remains were positioned with their caudal end toward the side of the structure where the fire was to be started (Figure 3.1). The position of the specimen relative to the fire allowed for the relationship between body position to the fire and the curvilinear fractures to be assessed.

Each burn consisted of a pair, hindlimbs or forelimbs, from a single specimen. Due to curvilinear fractures occurring in bones that have mainly reached the calcined phase, the bones were burned at temperatures between 600 and 940 degrees Celsius (Ellingham and Sandholzer, 2020; Shipman et al., 1984). The temperature of the fire was monitored every twenty minutes with a FLIR 8xt infrared detector that collects temperature data ranging from -4°F to 1022°F. This experiment took place in an outside environment and on different dates. The temperature, humidity, precipitation, and wind speed varied between the burn days. The varying temperatures and humidity inherently impacted the temperature the fire reached and the speed at which it was able to burn (MiKinley, 2006). Each burn consisted of the forelimb or hindlimbs representing one sheep and took between three to four hours to reach the desired calcined state. Because of the differing weights of the samples and the variable weather on the days, burn times varied (Table 3.1). Prior to lighting each fire, a baseline temperature and photos were taken to document the beginning state of the remains. The initial temperature information was documented on the first line of the data collection sheet (Table 3.2, Appendix A). Throughout each burn, detailed notes were made every twenty minutes. These notes included temperature of the fire, ambient temperature, any observed muscle shrinkage, progression of the fire, and amount of soft tissue left on the remains. The fire was put out by spraying water on the logs and ashes once the tissue surrounding tibiae and radii was mostly burned away and calcination was visible.

Once the remains cooled, they were transported to Anthropology Research Facility (ARF) and placed in wire cages to allow for the remaining soft tissue to decompose. Any fragments of bone that were not still encased in soft tissue were wrapped in foil and stored until they were cleaned. Once decomposition was mostly complete, the remains were transported from ARF to the lab and cleaned. Fragmented long bones were reassembled, barring lost fragments or warping, and glued together using Duco-cement. Reassembled bones and identified long bone fragments were then preserved using a 10% solution of Acryloid™ B-72 and acetone, based on the recommendation of Siegert and colleagues (2018). The solution was applied to each side of the burned bones using a soft brush and was allowed to dry before receiving two more coats.

Analysis

Post-burn and post-preservation, both the physical remains, video recordings, and observer notes were analyzed. Due to the limited sample size, the analysis was descriptive in nature, but a statistical model was calculated for what sample size would be needed to have a statistically significant sample for future research. The goal of this descriptive analysis was to assess whether curvilinear fractures are concave in the direction of the retreating tissue and whether the muscle tissue shrinking away from the heat can be observed in the recordings, which shows a potential correlation between the muscle shrinkage and the curvilinear fractures. The observation notes were compared to the video recordings for the accuracy of the observations. Each long bone was analyzed for the presence of curvilinear fractures (Table 3.3). Each curvilinear fracture present was documented, both written and photographically, based on individual sheep, limb, element, and the location of the fracture on the element. Concentric curvilinear fractures were counted together as a single instance. The initial fracture to occur in a set of curvilinear fractures can be identified as the first fracture on the convex side of the set (Pope, 2007). The key features notated in the descriptive analysis are the presence or absence of curvilinear fractures, the direction of the fracture's concavity, and if that

Table 3.3. Criteria used for scoring the presence or absence of curvilinear fractures and if they are convex distally.

Score	Presence/Absence of Curvilinear fracture	Score	Convex distally?
1	Present	1	yes
0	Absent	0	no
		n/a	Not applicable

concavity is in the direction of the receding muscle tissue. Other types of fractures were documented for the bones with observed curvilinear fractures and if the fracture interacted with the curvilinear fractures, then the chronology of fracture occurrence was discussed. In fracture analysis, it is possible to determine the sequence in which fractures occur based on how they interact with each other. If a fracture happened prior to other fractures, then all fractures that come in contact with them would terminate into the fracture as the energy dissipates along the existing fracture. Color and uniformity of burning was documented for each long bone. Each long bone was broken into fourths starting proximally and scored starting with the proximal fourth and ending at the distal fourth. Color was scored from unburned (1) to calcined (6) for each fourth of the bone. If multiple colors were present in the section being scored, the color that encompassed the majority received the score. This scoring system is based on descriptions outlined by Cain (2005) (Table 3.4). The uniformity of burning for each fourth of the long bone was recorded using a scoring system developed by Carroll and Smith (2018). Uniformity was scored from uniform (1) to five distinct patterns of burning (5) (Carroll and Smith, 2018) (Table 3.5). The uniformity score represents the number of colors that make up the burn pattern of the fourth being scored. Whether the bone surface is flat or curved where the curvilinear fractures fall was recorded along with any muscles that originate or insert on that location (May, 1970). Frequency data was calculated for the following: curvilinear presence or absence, direction of convexity, color score of fourth of bone with curvilinear fracture, uniformity score of fourth of bone with curvilinear fracture, and the bone surface for each fracture.

Normally, power analyses are performed *a priori* to determine the sample size needed to ensure that the model of choice has enough statistical power to reduce the likelihood of committing type II statistical error. However, this study serves only as a preliminary analysis and is limited in sample size. Therefore, a power analysis was performed *a posteriori* to determine the sample size needed to achieve the same effect size observed in this study under conditions characterized by different levels of statistical power. This approach provides an indirect way of evaluating how realistic the findings of this study

are by simulating study conditions that vary by sample size and statistical power (Cohen, 1992).

Table 3.4. Criteria used for identifying color of fragments by Cain 2005.

	Color	Description
1	Unburned	Off-white/cream/tan Brown/less than ½ carbonized
2	Dark brown	Dark brown/more than ½ carbonized
3	Black	Black/nearly fully carbonized
4	Grey	Grey/some white
5	Light grey	Light grey/bluish/more than ½ calcined
6	White	Fully calcined/white

Table 3.5. Criteria for uniformity scoring based on Carroll and Smith 2018.

Score	Uniformity
1	Complete Uniformity
2	Two patterns of burning
3	Three patterns of burning
4	Four patterns of burning
5	Five patterns of burning

CHAPTER FOUR

RESULTS

The following is the result of eight burns using the limbs from four sheep with a total of 16 limbs. Analyses will focus on 18 observed curvilinear fractures found on six radii, three ulnae, four metacarpals, one metatarsal, and four tibiae. It will begin with a discussion of qualitative observations before looking at frequency data.

Qualitative Observations

Each long bone was divided into fourths and analyzed from proximal to distal end. Each fourth was scored for primary color pattern and uniformity of color pattern using the scoring methods defined above (Table 4.1, Appendix B; Table 4.2, Appendix C; Table 3.4; Table 3.5). Burn pattern for each limb was documented on traced portions of a diagram that was credited to Marie-Pierre Coumont (Costamagno, et al. 2019). On the diagrams for the bones where curvilinear fractures were observed, all transverse and longitudinal fractures were documented. Below is a discussion of observations made during each burn and from watching the recorded burns, the extent of burning based on physical observation of the bones, and the presence of observed curvilinear fractures.

Specimen 2020-1 Forelimbs

The day this specimen was burned had an ambient temperature of 34°F, low or no wind, and high humidity. The burn lasted for a total of 80 minutes. Within the first ten minutes of the burn, both limbs curled cranially at the joint between the metacarpal and radius. The movement of the limbs occurred in small jerky shifts of the limb. As the limb curled further, the muscles of the shoulder were observed shifting laterally and flattening out, this could be due to shrinkage of the external shoulder muscles. The left limb progressed faster than the right, but by the end of 30 minutes, both had curled with a slight bend at the elbow joint (Figure 4.1). The tissue around the radius and metacarpal of both limbs then began to burn away, exposing the bone directly to the fire. For the remainder of the

Figure 4.1. Visual of the forelimbs curled cranially using 2020-3 Fore.

burn very little movement was observed. By the end of the burn, all exposed tissue was charred, most of the observable exposed bone was calcined, and a good portion of the shoulder muscles remained.

The bones of the right limb showed varying levels of burning, both between bones and within each individual bone (Table 4.1, Table 4.2, Figure 4.2). The humerus was only slightly charred on the distal end and the greater trochanter, and the metacarpal was mostly unburned, while the other bones of the limb show variable levels of burning. The proximal and distal fourth of the ulna are missing, but the remaining midshaft is mostly uniform in color, only showing two patterns of burning. The radius showed more patterns of burning across the bone, ranging from unburned and charred proximally to calcined distally. Both the radius and what is present of the ulna exhibit thermal fractures. The midshaft of the ulna was separated by several transverse fractures. The radius was slightly fragmented, with many transverse and longitudinal fractures. On the posterior of the proximal end are two concentric curvilinear fractures run that along the zone of pyrolysis, sometimes referred to as the heat line (Table 4.3, Table 4.4). The zone of pyrolysis is a distinguishable area that falls between burned and unburned bone. It is often slightly dark brown or tan in color. The bone in between the two fractures was lost in the burn. The surface of the bone at the location of the curvilinear fractures was flat and several muscles insert and originate on the general location of the fractures. The biceps brachii and the brachialis both insert onto the interosseus ligament (May, 1970) (Figure 3.1). The extensor digitorum communis originates on the interosseus ligament and the bone around the ligament. On the lateral tuberosity the extensor digitorum lateralis originates (May, 1970) (Figure 3.1). The curvilinear fractures are concave towards the proximal end (Figure 4.3). Only one fracture came into contact with the curvilinear fractures. A single longitudinal fracture terminates into the first curvilinear fracture of the set. This shows that a curvilinear fracture occurred prior to the longitudinal fracture occurring.

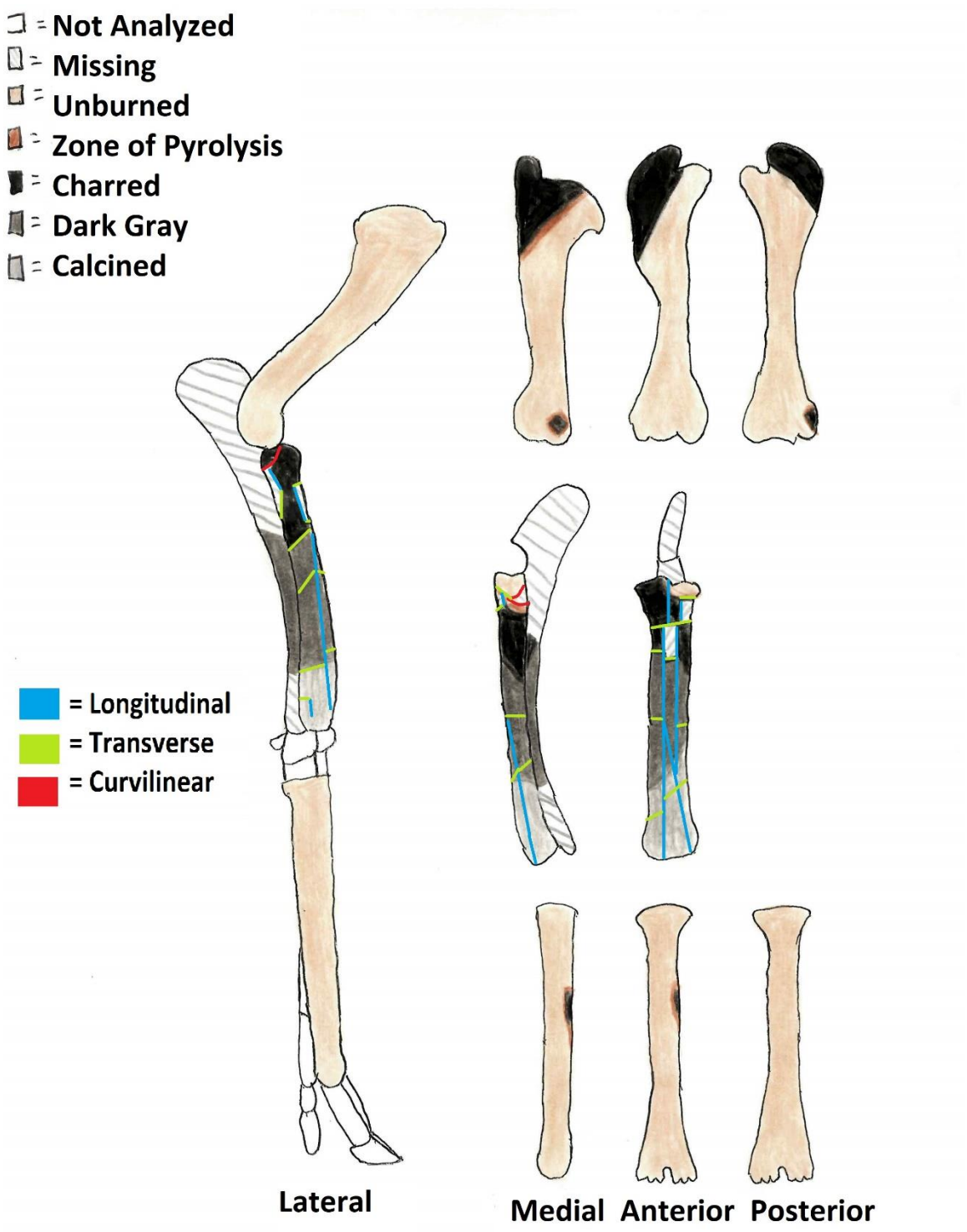

Figure 4.2. Diagram depicting the degree of burning of 2020-1 Right Forelimb.

Table 4.4. Fourth of bone, color score, uniformity score, and bone surface shape for all the curvilinear fractures of 2020-1.

Specimen	Limb pair	Side/Element	Location	1/4 of bone	Color Score	Uniformity Score	Bone Surface
2020-1	Fore	Left/Radius	Posterior midshaft	2	3	4	flat
2020-1	Fore	Right/Radius	Posterior Proximal end	1	3	2	flat
2020-1	Fore	Left/Ulna	Posterior midshaft	2	3	1	flat

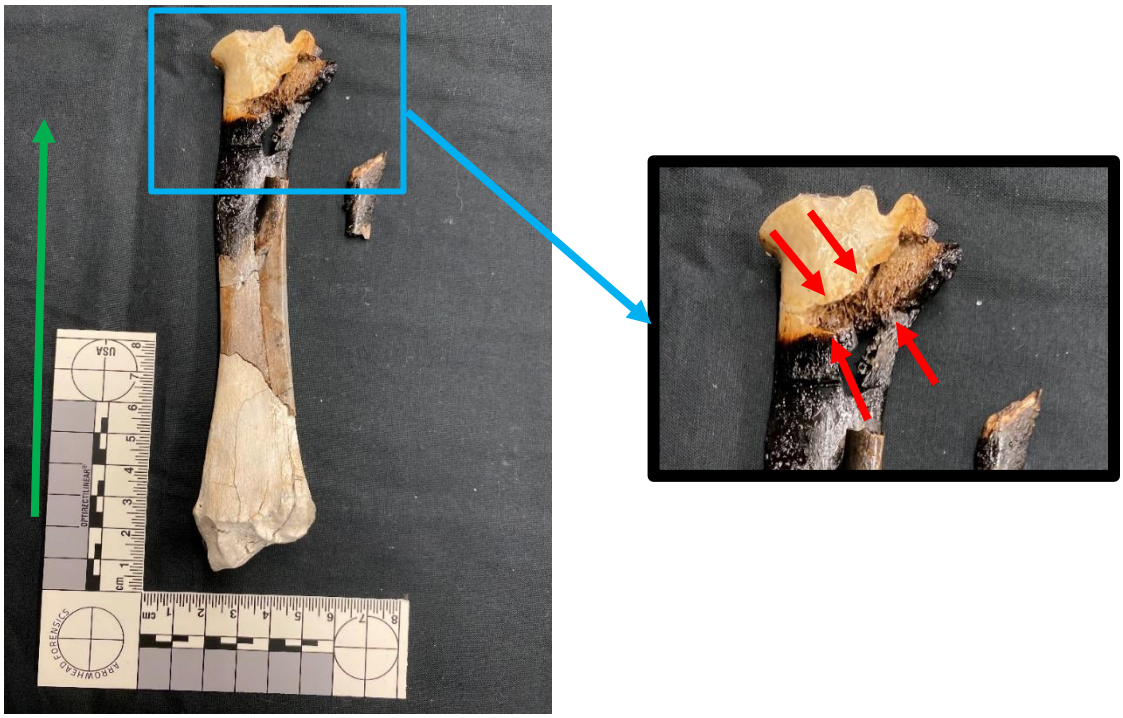

Figure 4.3. 2020-1 posterior view of the right radius, up close image of curvilinear fracture indicated by red arrows. The proximal end of the bone is at the top of the picture. The green arrow indicates the direction that the bone was burned.

Similar to the right limb, the bones of the left forelimb showed varying levels of burning (Table 4.1, Table 4.2, Figure 4.4). The humerus was mostly unburned. Proximally the radius and ulna were unburned, and the metacarpal was unburned distally. The metacarpal was charred on the majority of the shaft, and only two patterns of burning were observed in each fourth of the bone. The ulna was similar in uniformity to the metacarpal, but the burned portions of the radius and the ulna both ranged from charred to calcined. Unlike the ulna and metacarpal, the radius has three to four patterns of burning per fourth of bone. Unsurprisingly, due to the extensive burning of the radius, it was also highly fragmented, particularly the anterior surface. Many longitudinal and transverse fractures come together to create an almost checkered fragmentation of the anterior surface. The posterior surface was mainly unfractured, barring a single curvilinear fracture on the midshaft along the divide between the dark gray and charred portions of the bone (Table 4.3, Table 4.4, Figure 4.5). The curvilinear fracture was concave proximally and was mirrored on the ulna. The ulna has an unburned proximal third, charred medially, and calcined on the distal end. The surface of both bones where the fracture occurred is flat and the extensor digitorum communis attaches there to both bones (May, 1970) (Figure 3.1). The fracture on the ulna comes into contact with no other fractures, but a single longitudinal fracture terminates into the curvilinear fracture on the radius superiorly.

Specimen 2020-1 Hindlimbs

The day of the burn had an ambient temperature of 52°F, high winds, and average humidity. Due to the high winds, the burn took 300 minutes. While observing the burn, no movement could be seen in the first 20 minutes, but when the video recordings were observed at a sped-up rate, the slight extension of both limbs were observed. Both limbs continued to slowly extend before shifting medially. After an hour, the limbs began to shift laterally, and the left limb began to curl cranially. The left limb snapped at the tibia as the right limb shifted further laterally. No movement was observed for the next hour except the slight movement of the muscles of the hips laterally. The right limb eventually began to shift anteriorly, and the hip muscles shifted laterally, causing the limbs to move

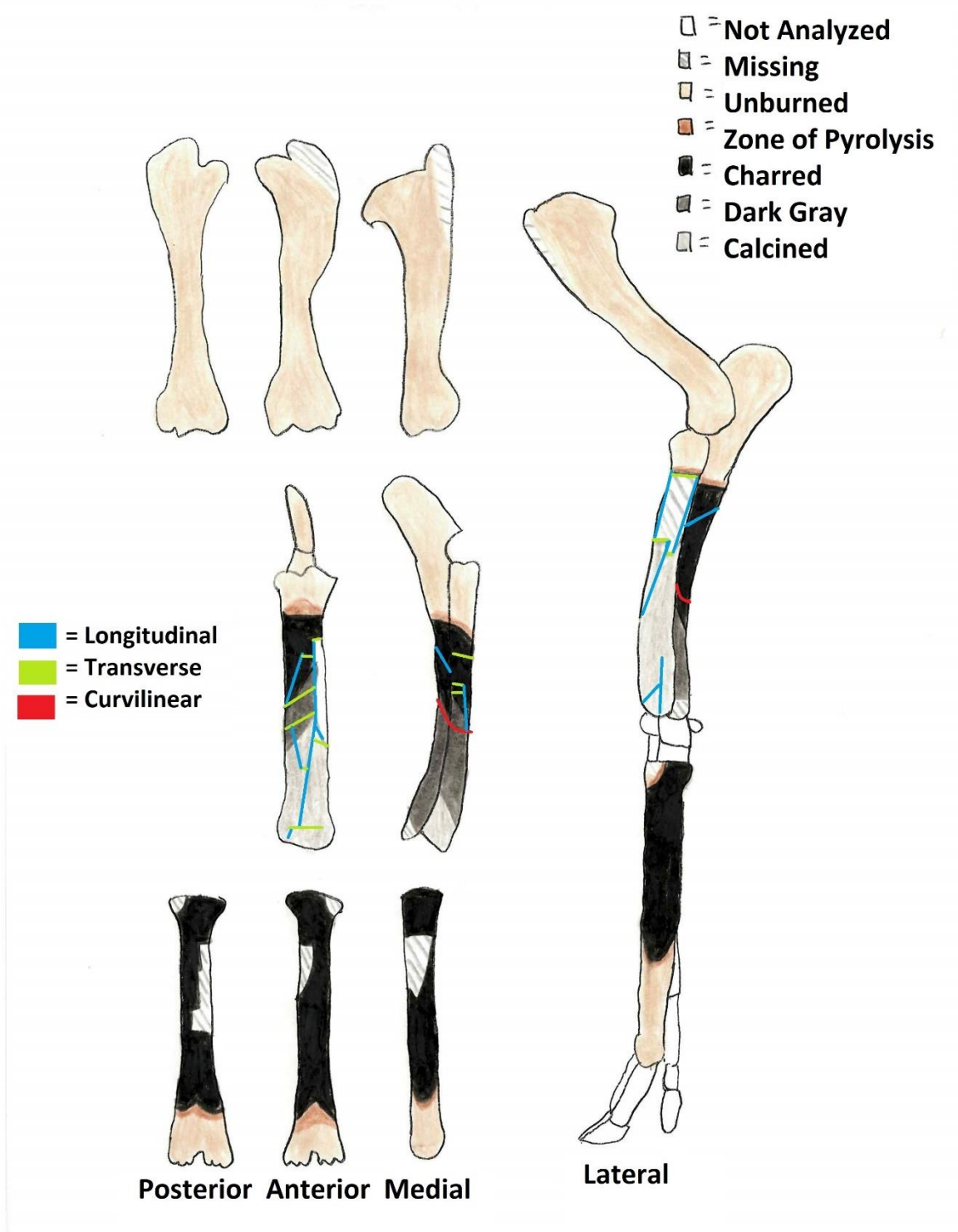

Figure 4.4. Diagram depicting the degree of burning of 2020-1 Left Forelimb.

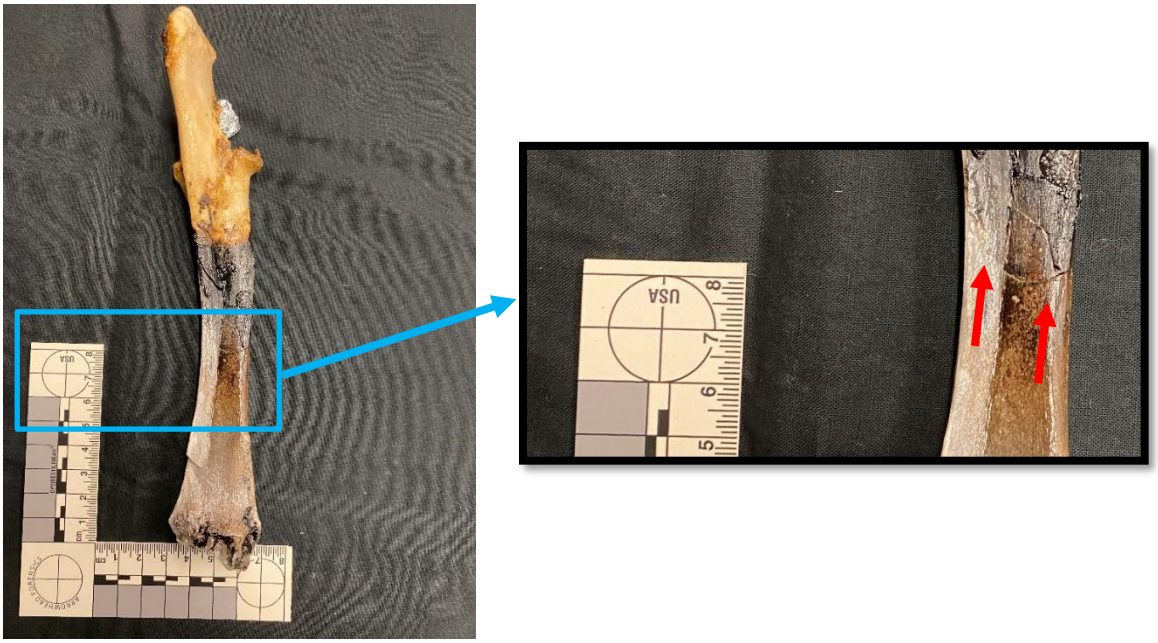

Figure 4.5. 2020-1 posterior view of articulated left ulna and radius, up close image of curvilinear fracture. The proximal end of the bone is at the top of the picture. Red arrows indicate the fractures. The green arrow indicates the direction that the bone was burned.

slightly. For the remainder of the burn, the only movement observed is the curling of the spine dorsally.

All but two of the bones from the hind limb of this specimen remain mostly unburned (Table 4.1, Table 4.2, Figure 4.6, Figure 4.7). Though only the right metatarsal remained completely unburned. Both femora and the right tibia, while mostly unburned, all had slight charring on different portions. The left tibia was primarily charred with an unburned proximal end and two to three patterns of burning per section. The left metacarpal was mostly charred on the proximal half and mainly dark gray distally, though the distal half showed four patterns of burning per fourth. While both bones were slightly fragmented with few longitudinal and transverse fractures, neither bone had a curvilinear fracture (Table 4.3).

Specimen 2020-2 Forelimbs

The ambient temperature at the start of the burn was 37°F with low to no wind and average humidity. The duration of the burn was 80 minutes. Within the first 10 minutes of the burn, the left limb began to curl at the distal joint and, by the end of 25 minutes, had curled inward completely. The right limb curled slowly inward, and the internal muscles of the right shoulder began to contract. The right limb curled completely inward, and the muscles of both shoulders contracted dorsally, flattening them. No further movement was observed for the remainder of the burn.

All of the bones of the right limb showed extensive burning with very little bone left unburned (Table 4.1, Table 4.2, Figure 4.8). None of the bones were uniformly burned, all showed three or more patterns of burning per fourth. Calcination was the major burn pattern of the radius, and it was slightly fragmented anteriorly with a few fractures posteriorly. There were seven concentric curvilinear fractures on the posterior, starting around midshaft and moving proximally (Figure 4.9, Table 4.5). The curvilinear fractures were concave proximally (Table 4.3). The surface of the bone where the fracture falls is

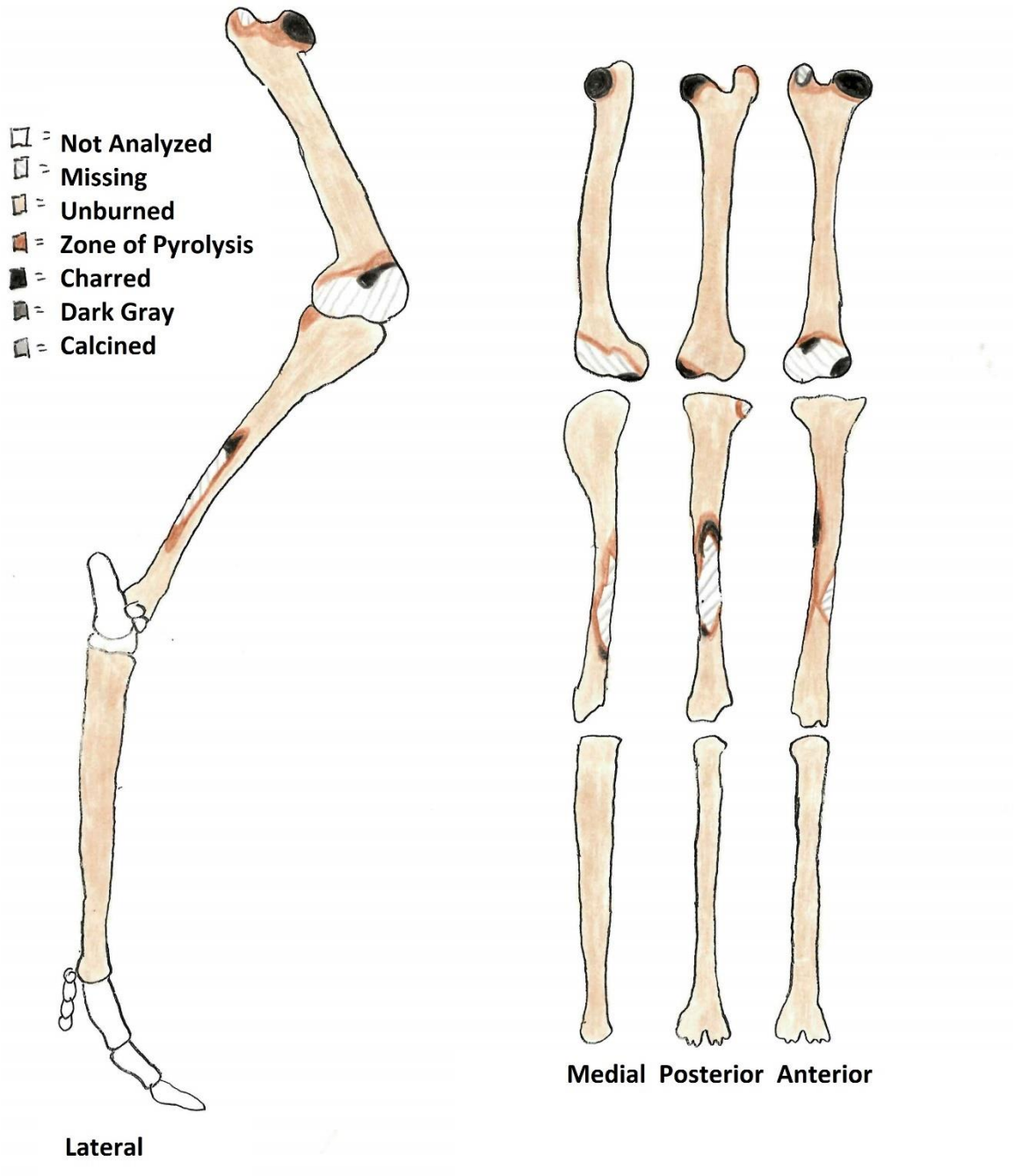

Figure 4.6. Diagram depicting the degree of burning of 2020-1 Right Hindlimb.

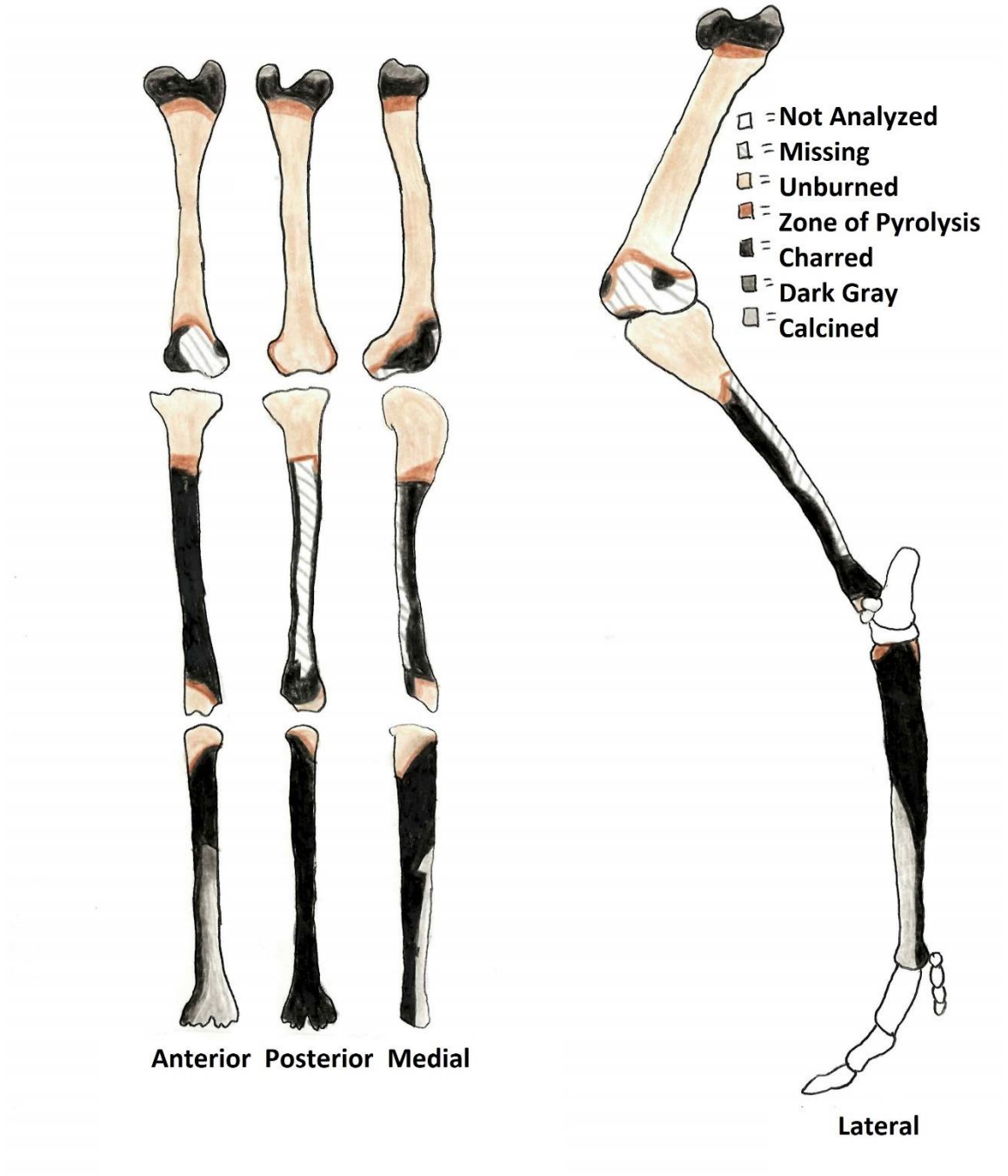

Figure 4.7. Diagram depicting the degree of burning of 2020-1 Left Hindlimb.

Table 4.5. Fourth of bone, color score, uniformity score, and bone surface shape for all the curvilinear fractures of 2020-2.

Specimen	Limb pair	Side/Element	Location	1/4 of bone	Color Score	Uniformity Score	Bone Surface
2020-2	Fore	Right/Metacarpal	Posterior Distal shaft	4	3	3	flat
2020-2	Fore	Left/Radius	Posterior Proximal midshaft	1	4	5	flat
2020-2	Fore	Right/Radius	Posterior midshaft	2	5	3	flat
2020-2	Fore	Left/Ulna	Medial midshaft	2	4	4	curved
2020-2	Hind	Left/Tibia	Lateral Posterior midshaft	3	3	4	curved
2020-2	Hind	Right/Tibia	Lateral midshaft	3	3	3	curved

flat and the biceps brachii, brachialis, extensor digitorum lateralis, and extensor digitorum lateralis all attach to the bone in that area (May, 1970) (Figure 3.1). Along the lateral edge of the posterior shaft is a deep longitudinal fracture that all of the curvilinear fractures terminate into, meaning that the curvilinear fractures occurred after the longitudinal fracture occurred (Figure 4.9). The metacarpal was primarily charred but was slightly calcined posteriorly. It had a few longitudinal and transverse fractures. On the posterior surface, there was a set of concentric curvilinear fractures falling in the charred bone and the zone of pyrolysis that were concave distally (Figure 4.10, Table 4.5). The surface on which the curvilinear fractures occurred is flat and the flexor digitorum superficialis attached in the general area the fractures occurred (May, 1970) (Figure 4.3). The curvilinear fractures terminate into a short longitudinal fracture on the medial surface, a longitudinal fracture terminates into the first curvilinear fracture of the set, and a transverse fracture terminates into the second fracture of the concentric set. This means that the longitudinal fracture on the medial shaft occurred prior to the curvilinear fractures, but the curvilinear fractures occurred prior to the longitudinal and transverse fractures that terminate into them.

Compared to the right limb, the left limb had much more unburned bone, but no bone remained entirely unburned (Table 4.1, Table 4.2, Figure 4.11). The humerus was mostly unburned, but each portion of the bone was partially charred. Similarly, the metacarpal was unburned distally and partially charred proximally. The burning of the radius was highly variable with very low uniformity and calcination and light gray as the major colors present. The shaft of the radius was highly fragmented, extensively on the anterior surface, with a combination of longitudinal and transverse fractures. On the posterior surface, there were several spaced-out curvilinear fractures moving proximally (Figure 4.12, Table 4.5). These curvilinear fractures were concave proximally (Table 4.3). Like the previous curvilinear fractures on the posterior radial shaft, the bone surface is flat, and several muscles attach on the surface. The ulna was also mostly calcined but was slightly more uniform in burn pattern, with the distal fourth entirely calcined. It has several transverse fractures along the calcined shaft, and the medial portion of the proximal end

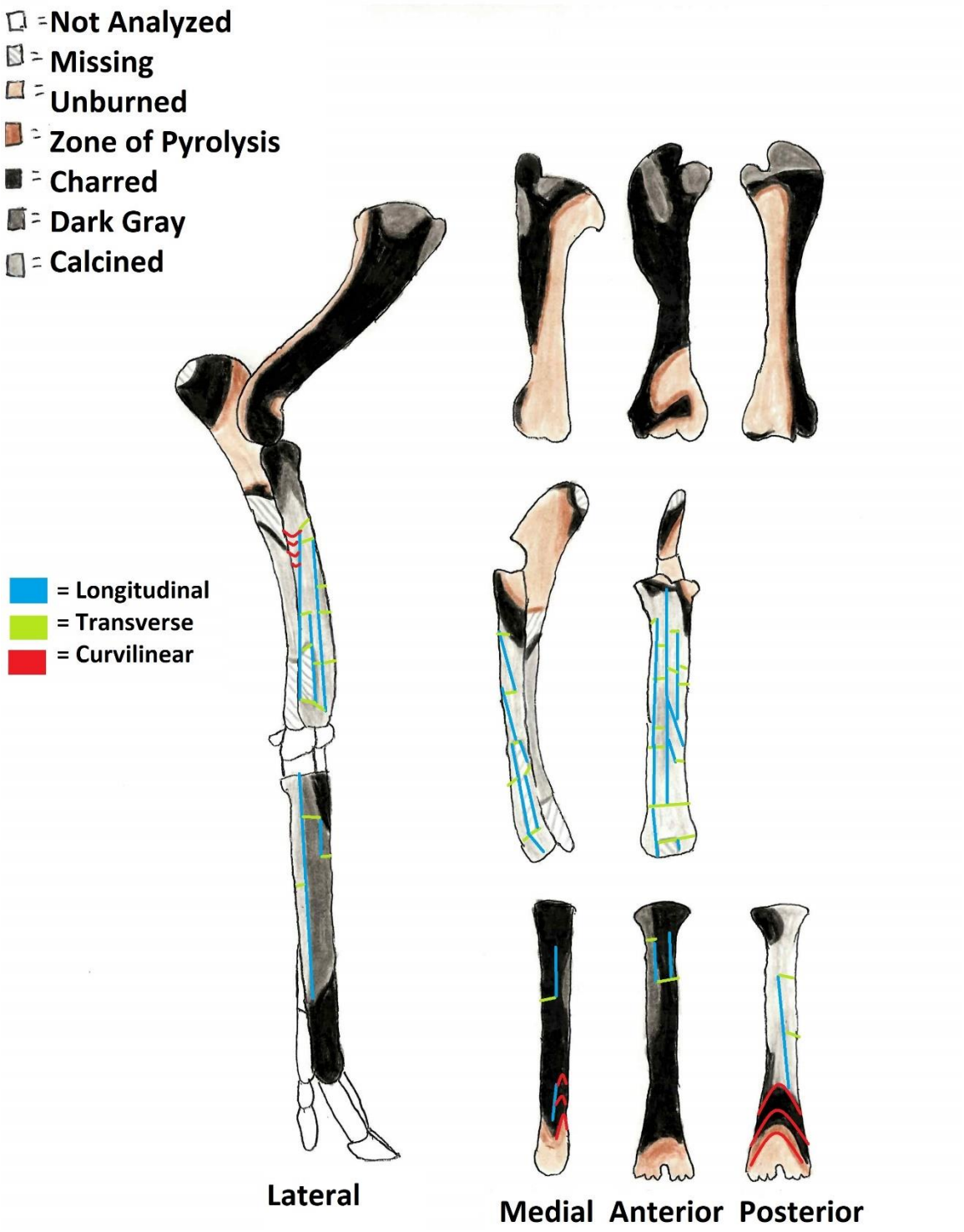

Figure 4.8. Diagram depicting the degree of burning of 2020-2 Right Forelimb.

Figure 4.9. 2020-2 posterior view of the right radius with visible concentric curvilinear fractures. The proximal end of the bone is at the **top** of the picture. Red arrows indicated the first fracture in the set of curvilinear fractures. Yellow arrows indicate a few of the subsequent concentric curvilinear fractures. The green arrow indicates the direction that the bone was burned.

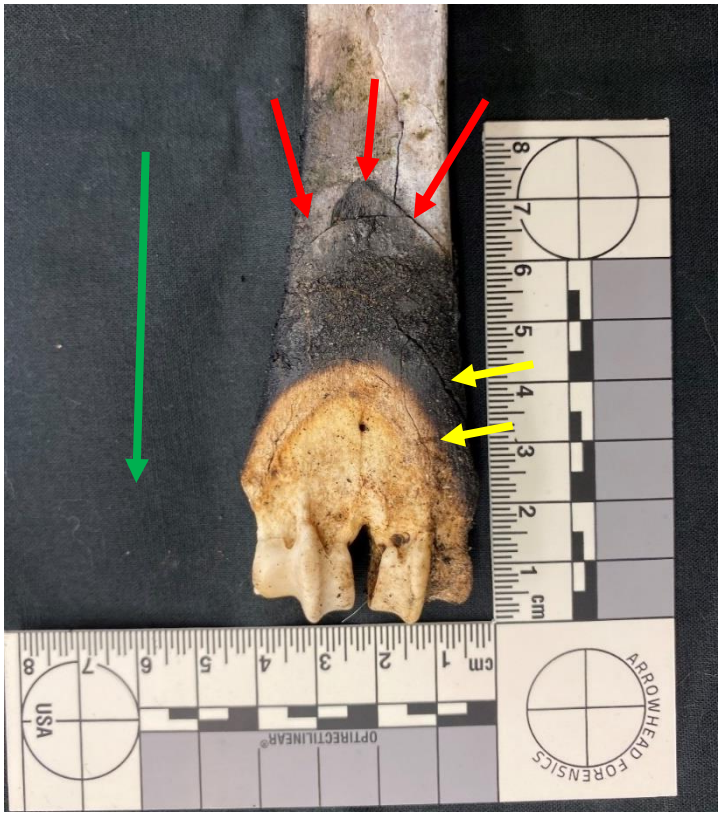

Figure 4.10. 2020-2 posterior view of the right metacarpal with visible concentric curvilinear fractures. The proximal end of the bone is at the top of the picture. Red arrows indicated the first fracture in the set of curvilinear fractures. Yellow arrows indicate the subsequent concentric curvilinear fractures. The green arrow indicates the direction that the bone was burned.

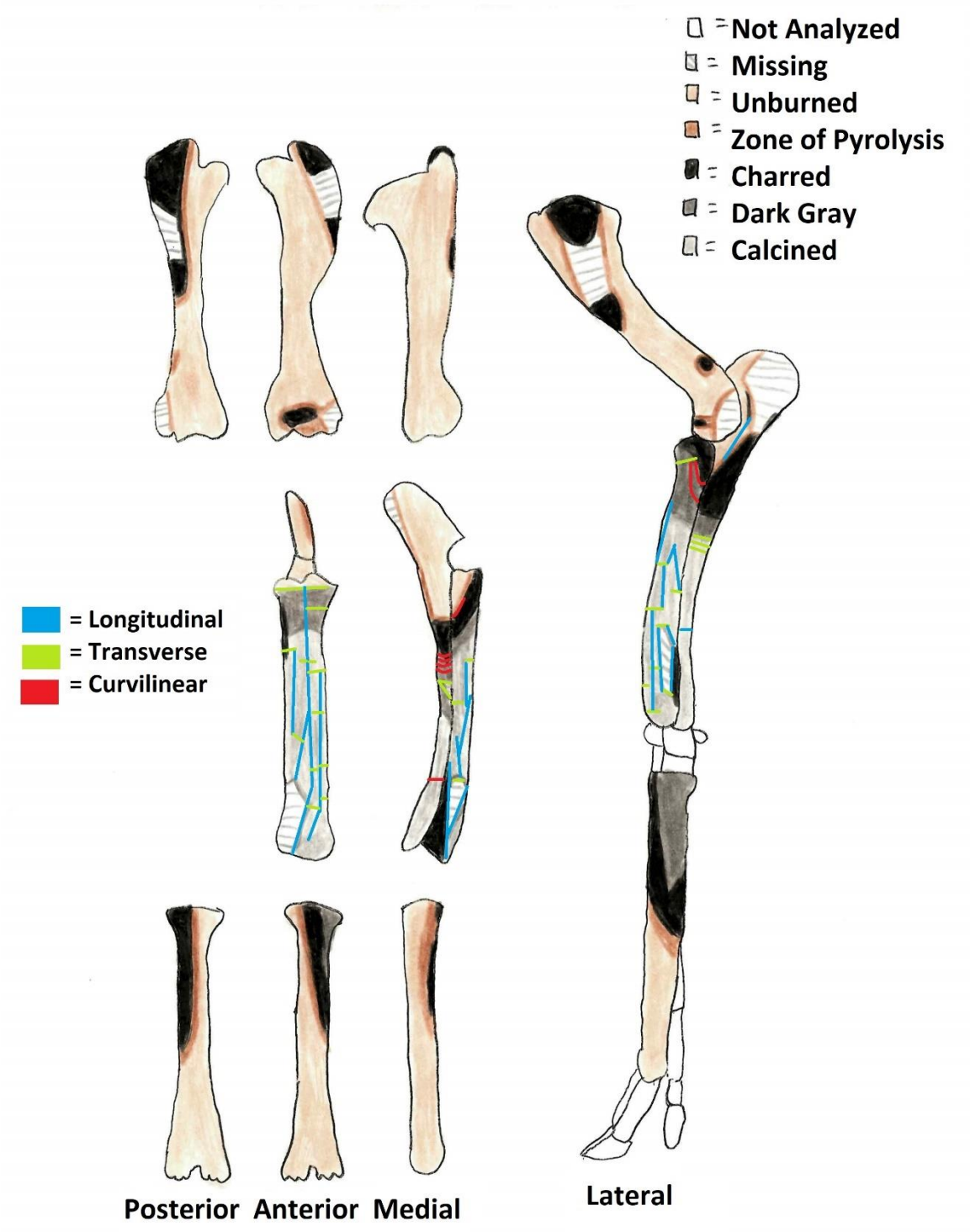

Figure 4.11. Diagram depicting the degree of burning of 2020-2 Left Forelimb.

Figure 4.12. 2020-2 posterior view of the left radius with concentric curvilinear fractures. The proximal end of the bone is at the top of the picture. Red arrows indicated the first fracture in the set of curvilinear fractures. Yellow arrows indicate the subsequent concentric curvilinear fractures. The green arrow indicates the direction that the bone was burned.

was detached. On the medial edge at midshaft in the border of the dark gray and charred bone was a set of several concentric curvilinear fractures (Figure 4.13, Table 4.5). These fractures were concave proximally (Table 4.3). The fractures wrap around the curved edge of the bone and three muscles attach in that location. The brachialis, biceps brachii, extensor digitorum communis, and abductor pollicis longus all originate or insert on the bone in this area. No other fractures came in contact with the curvilinear fractures.

Specimen 2020-2 Hindlimbs

The ambient temperature at the start of the burn was 26°F with low to no wind and average humidity. The duration of the burn was 140 minutes. Due to logistics, the camera was unavailable for the burn of this specimen, so the following is based on the observer notes. No movement was observed in the first hour of the burn. The left limb was the first to be observed moving and was seen starting to curl inwards as the muscles of the hips began to burn. The bones of the left limb were exposed and visibly calcined before the limb fell after the tissue holding the metatarsal in place broke. There was no observable movement in the right limb for the first 80 minutes of the burn, but the limb began to curl cranially. The muscles surrounding the tibia was burning, while there is little change to the distal limb. At the end of the burn, the right limb had also fallen and was visibly calcined.

The bones of the left limb were variably burned (Table 4.1, Table 4.2, Figure 4.14). The femur remained mostly unburned, barring slight charring on the distal end. The metatarsal and distal tibia were extensively burned, ranging from charred to calcined. Proximally the tibia was mainly unburned but exhibited slight charring. Both the tibia and the metatarsal were highly fragmented with longitudinal and transverse fractures. Though the tibia was the only bone of the left limb on which curvilinear fractures were observed (Table 4.3, Table 4.5). On the lateral posterior edge at midshaft, there were two concentric curvilinear fractures that were concave proximally. The curvilinear fractures wrap around the curved lateral edge of the bone where no muscles insert or originate

Figure 4.13. 2020-2 medial view of the left ulna with shallow concentric curvilinear fractures indicated by a red arrow. The proximal end of the bone is at the top of the picture. The green arrow indicates the direction that the bone was burned.

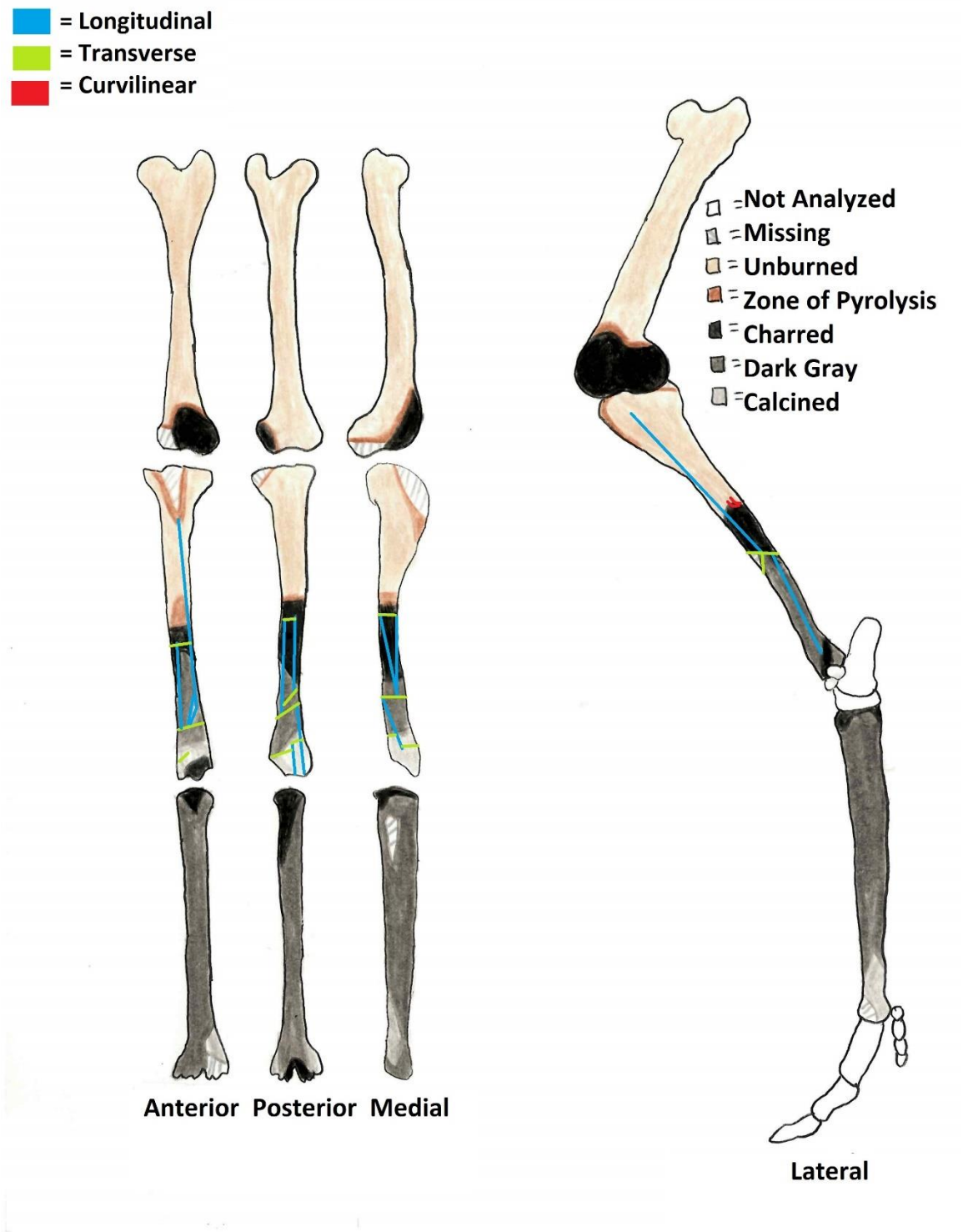

Figure 4.14. Diagram depicting the degree of burning of 2020-2 Left Hindlimb.

(May, 1970) (Figure 3.1). The curvilinear fractures both terminated into a longitudinal fracture, meaning the longitudinal fracture occurred first.

Unlike the bones of the left limb, the bones of the right limb were mostly unburned (Table 4.1, Table 4.2, Figure 4.15). The femur had slight charring proximally, and the distal end was mainly charred but with four other patterns of burning. Similarly, the metatarsal was mostly unburned with slight charring along the proximal three-fourths. The tibia had the most extensive burning of the limb, though the proximal half was mostly unburned, barring slight charring. Distally the tibia was primarily charred, with calcination on the lateral, posterior, and medial distal fourth. The distal end of this bone was slightly fragmented and had several longitudinal and transverse fractures. A set of four concentric curvilinear fractures was observed along the lateral midshaft in the zone of pyrolysis (Figure 4.16, Table 4.5). They were concave proximally and on a curved surface (Table 4.3). Several muscles originate and insert on the lateral anterior midshaft of the bone, they are the tibialis cranialis, semitendinosus, tensor fasciae latae, biceps, femoris (May,1970) (Figure 3.1).

Specimen 2020-3 Forelimbs

The ambient temperature at the start of the burn was 36°F with high winds and average humidity. The duration of the burn was 160 minutes. For the first 20 minutes of the burn, there was no observable movement. Both limbs then began to curl cranially, the right limb progressing faster than the left. As the limbs continued to curl inward, the muscles of the shoulders were seen contracting dorsally, causing the shoulders to flatten out. By the end of 80 minutes both limbs had curled completely inward and exposed charred and calcined bone was observed on both limbs.

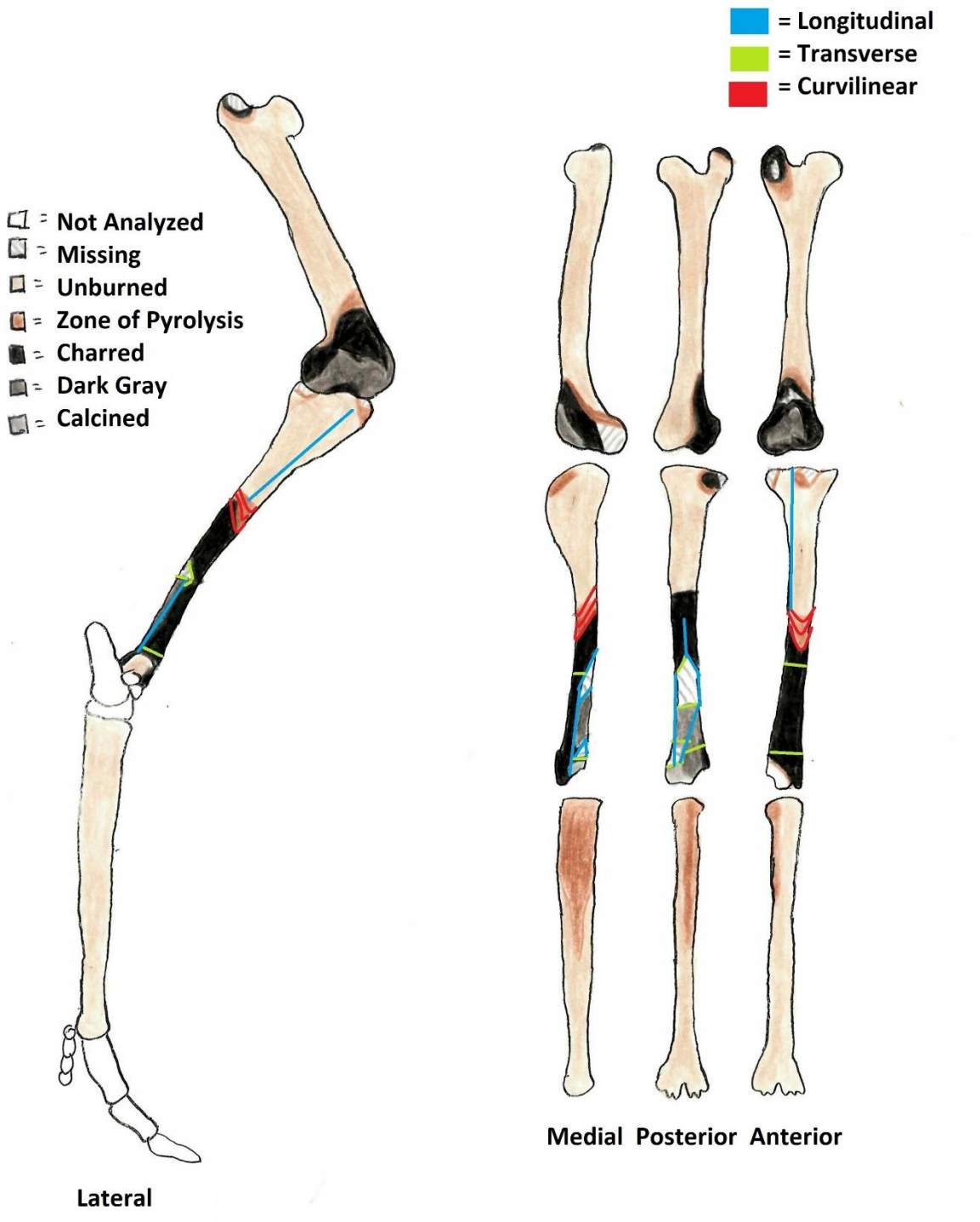

Figure 4.15. Diagram depicting the degree of burning of 2020-2 Right Hindlimb.

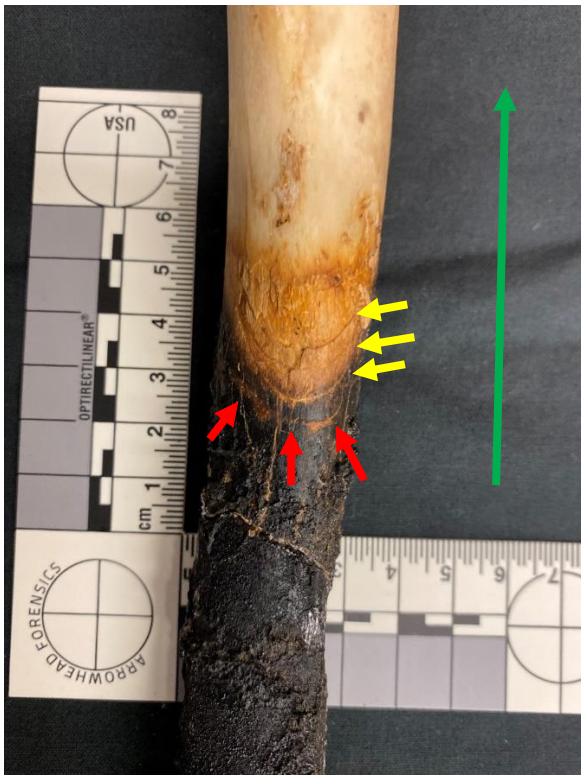

Figure 4.16. 2020-2 lateral view of the right tibia with concentric curvilinear fractures. The proximal end is on the top of the picture. Red arrows indicated the first fracture in the set of curvilinear fractures. Yellow arrows indicate the subsequent concentric curvilinear fractures. The green arrow indicates the direction that the bone was burned.

The bones of the left limb were mostly unburned (Table 4.1, Table 4.2, Figure 4.17). The ulna was completely unburned, but the distal fourth is missing. Both the humerus and the metacarpal were unburned, barring slight charring and zones of pyrolysis, though the metacarpal was highly fragmented with the majority of the lateral shaft absent. The radius was the most extensively burned of the limb. Bone was missing from both the posterior and anterior shaft. What was present of the proximal end was unburned, barring a zone of pyrolysis around the edge with slight delamination. Distally, what was left of the radius showed many patterns of burning from calcination laterally to an unburned medial edge. None of the bones of the left limb exhibited curvilinear fractures (Table 4.3).

Compared to the mostly unburned left limb, the right limb was extensively burned (Table 4.1, Table 4.2, Figure 4.18). The humerus was the least burned of the limb, with only slight charring on the proximal and distal ends. The remaining three bones all had low uniformity, and their patterns included various stages of burning from unburned to calcined. The ulna was missing its distal half and had only one longitudinal and two transverse fractures. Both the radius and metacarpal were highly fragmented with missing bone. On the lateral posterior proximal end of the radius, several concentric curvilinear fractures were observed in the charred bone and zone of pyrolysis. A fragment of bone was missing between two of the observed fractures (Figure 4.19, Table 4.6). These curvilinear fractures were concave proximally (Table 4.3). Resembling the previous radii, the fractures fell on the flat posterior radial shaft where several muscles attach (May, 1970) (Figure 3.1). Concentric curvilinear fractures all terminated into a transverse fracture laterally and a longitudinal fracture terminated into the first curvilinear fracture.

Specimen 2020-3 Hindlimbs

The ambient temperature at the start of the burn was 36°F, and the weather included high winds and average humidity. The burn lasted 180 minutes. This specimen was placed on its left side due to the position in which it froze. Both limbs began to curl cranially within the first 20 minutes of the burn. The left leg progressed faster and curled completely

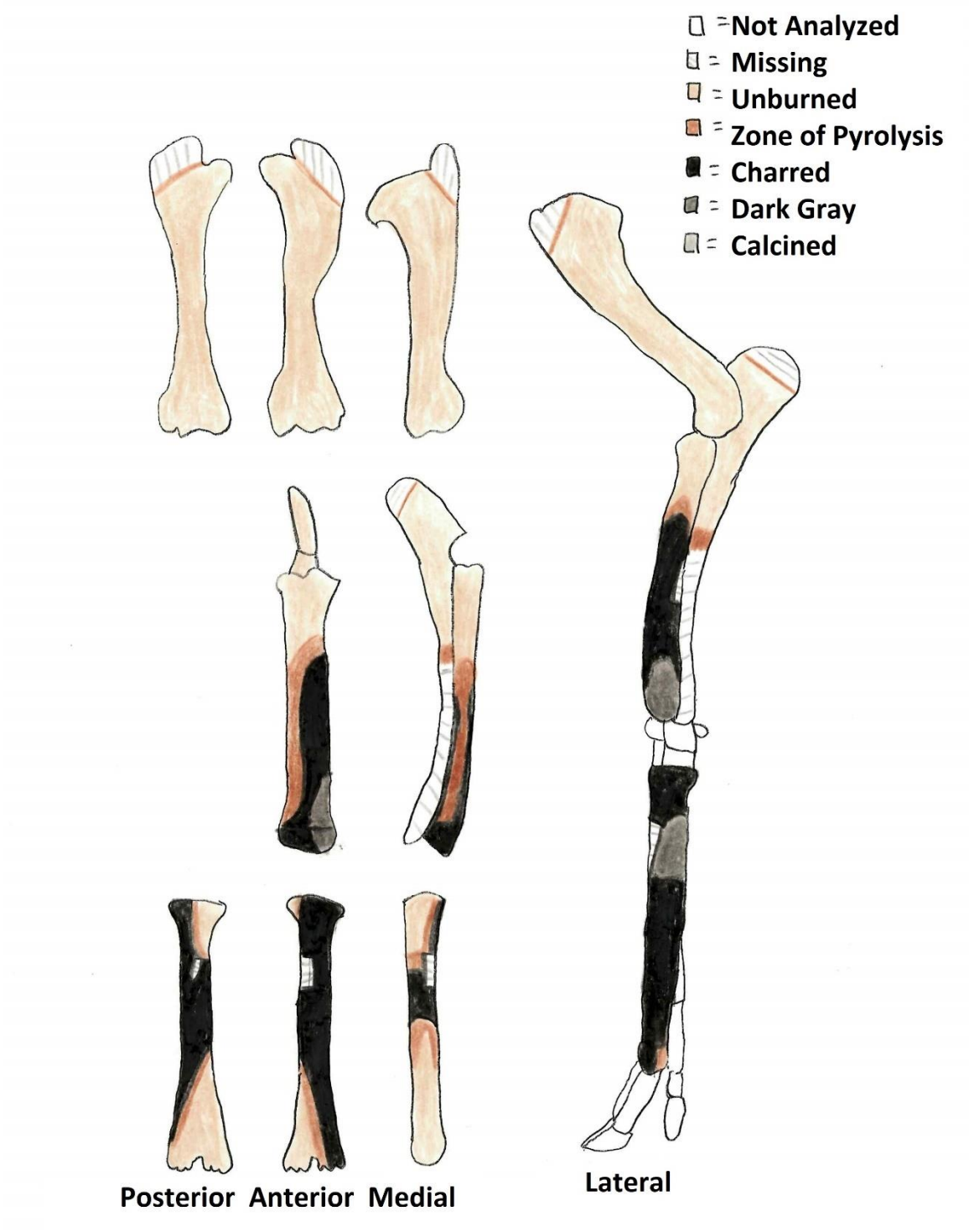

Figure 4.17. Diagram depicting the degree of burning of 2020-3 Left Forelimb.

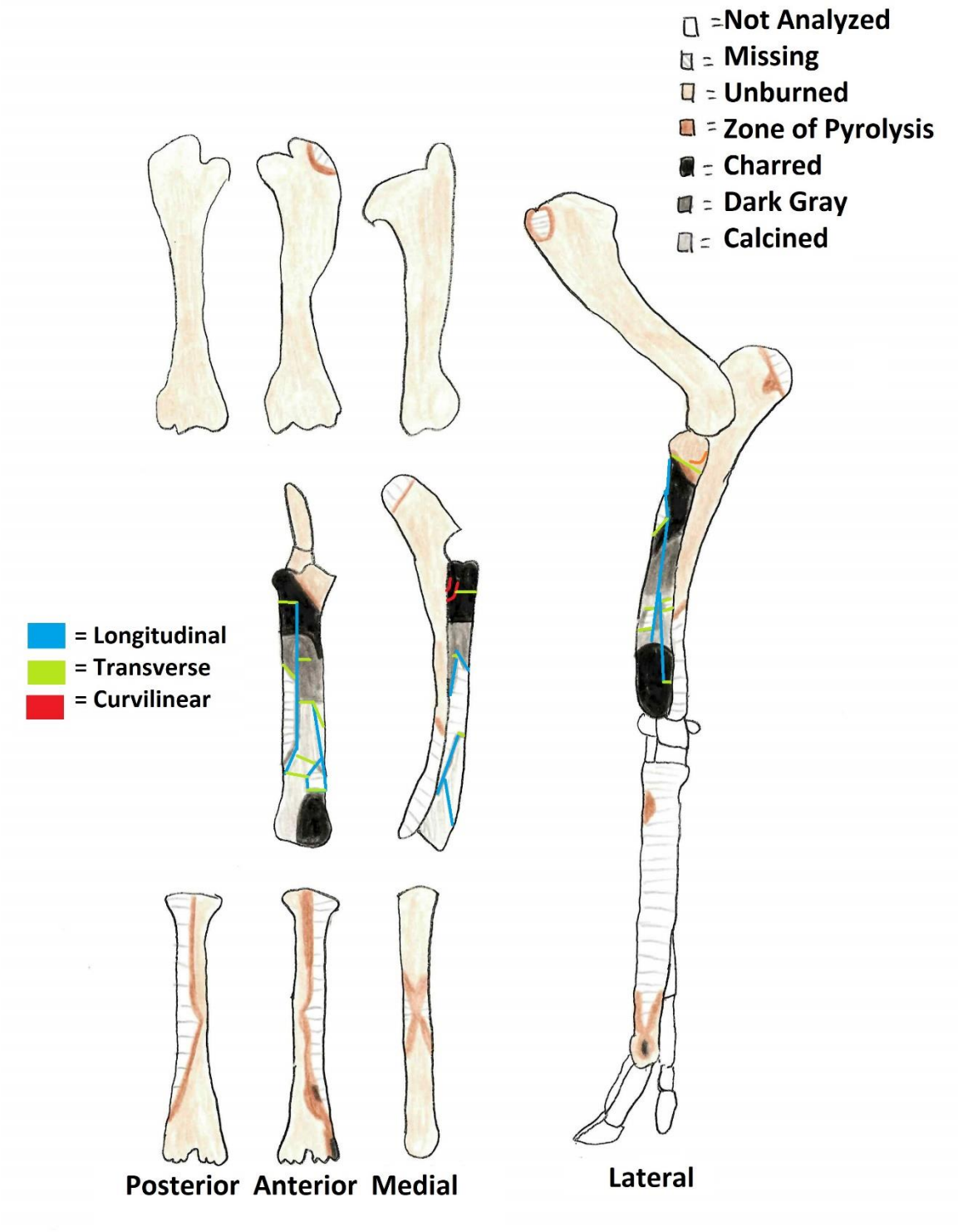

Figure 4.18. Diagram depicting the degree of burning of 2020-3 Right Forelimb.

Figure 4.19. 2020-3 posterior view of the right radius with concentric curvilinear fractures. The proximal end of the bone is on the top of the picture. Red arrows indicated the first fracture in the set of curvilinear fractures. Yellow arrows indicate the subsequent concentric curvilinear fractures. The green arrow indicates the direction that the bone was burned.

Table 4.6. Fourth of bone, color score, uniformity score, and bone surface shape for all the curvilinear fractures of 2020-3.

Specimen	Limb pair	Side/Element	Location	1/4 of bone	Color Score	Uniformity Score	Bone Surface
2020-3	Fore	Right/Radius	Posterior Proximal end	1	3	3	flat
2020-3	Hind	Left/Tibia	Posterior midshaft	2	4	4	curved

cranially by the end of 40 minutes (Figure 4.20). When the right leg began to curl cranially, the left limb was seen fracturing and falling. The right limb did not curl completely inward before it fractured and fell. Little to no movement was seen in the muscles of the haunch throughout the entire burn.

Like many of the previously discussed specimens, the right femur was mostly unburned besides slight charring on the distal end. The remaining two bones of the right limb showed more extensive burning, each fourth showed many patterns of burning (Table 4.1, Table 4.2, Figure 4.21). Though charring was the primary color pattern present on both. Both bones were highly fragmented with several longitudinal and transverse fractures, but neither exhibited curvilinear fractures (Table 4.3).

Like the right femur, the left femur was mainly unburned, barring the distal end, but the burning to the distal end of the left was less uniform, and the primary color pattern observed was dark gray (Table 4.1, Table 4.2, Figure 4.22). The metatarsal's burning ranged from unburned to light gray and had several longitudinal and transverse fractures. Similarly, the tibia showed many patterns of burning and was mainly charred. The shaft of the tibia was highly fragmented and was missing a portion of the proximal end. On the posterior side of the tibia around the midshaft, there were several shallow concentric curvilinear fractures that were both concave proximally (Figure 4.23, Table 4.3, Table 4.6). The fractures fell on the curved lateral posterior shaft where the popliteus muscles inserts (May, 1970) (Table 4.6, Figure 3.1). On the posterior surfaces there was a longitudinal fracture in which all the curvilinear fractures terminated.

Specimen 2020-4 Forelimbs

The ambient temperature at the start of the burn was 36°F with high winds and average humidity. Both the night before and the morning of the burn, a mix of rain and snow occurred in Morgan County, where the burn site is located. This made the ground, burn structure, and wood damp and slightly cold. The duration of the burn was 180 minutes.

Figure 4.20. Visual example of the hind limb curling cranially using 2020-4 Hind. The left limb towards the back of the structure is a good representation of the stopping place of the hindlimbs in the sample. Though other limbs did curl slightly further cranially, no other visuals were as clear.

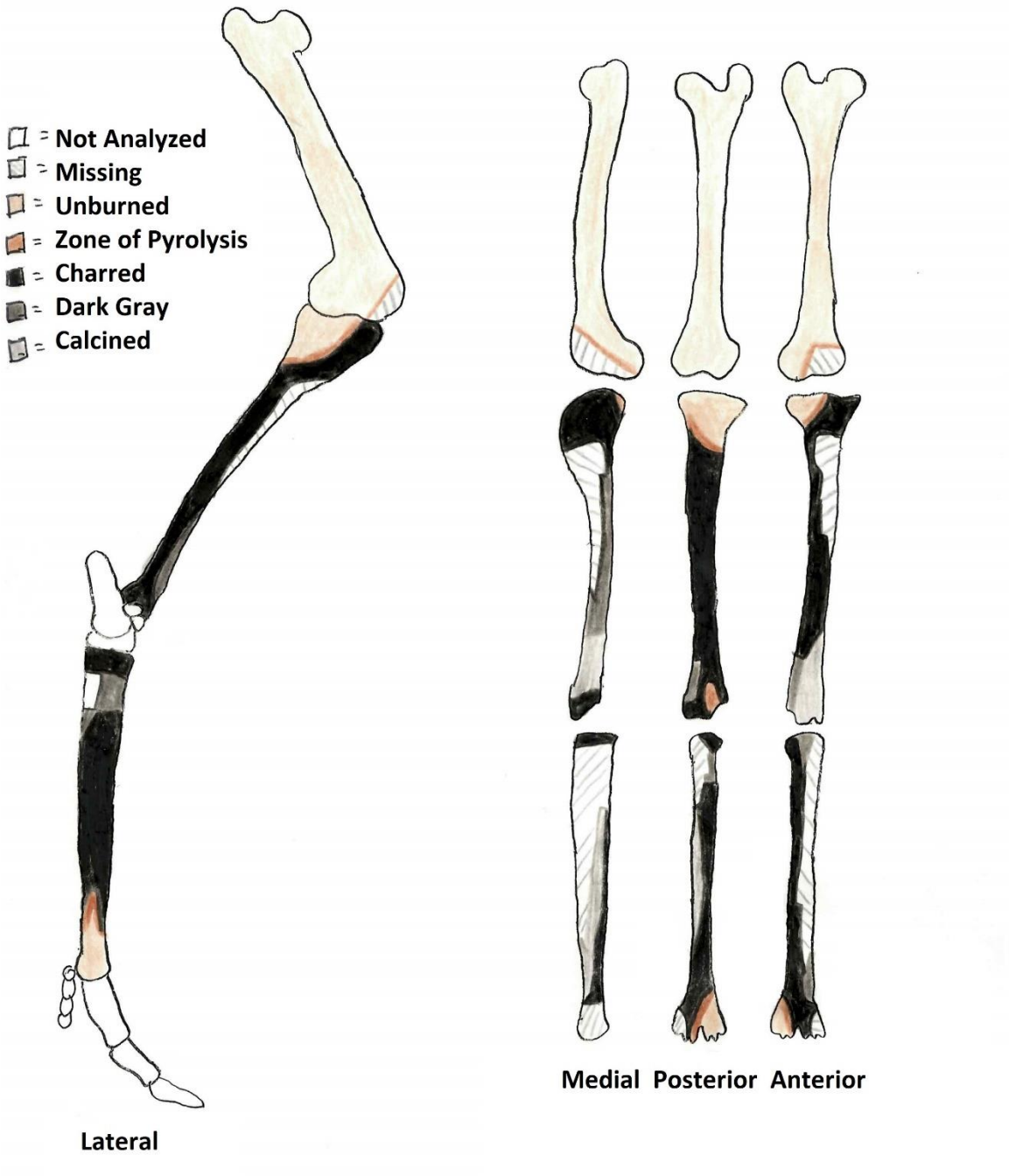

Figure 4.21. Diagram depicting the degree of burning of 2020-3 Right Hindlimb.

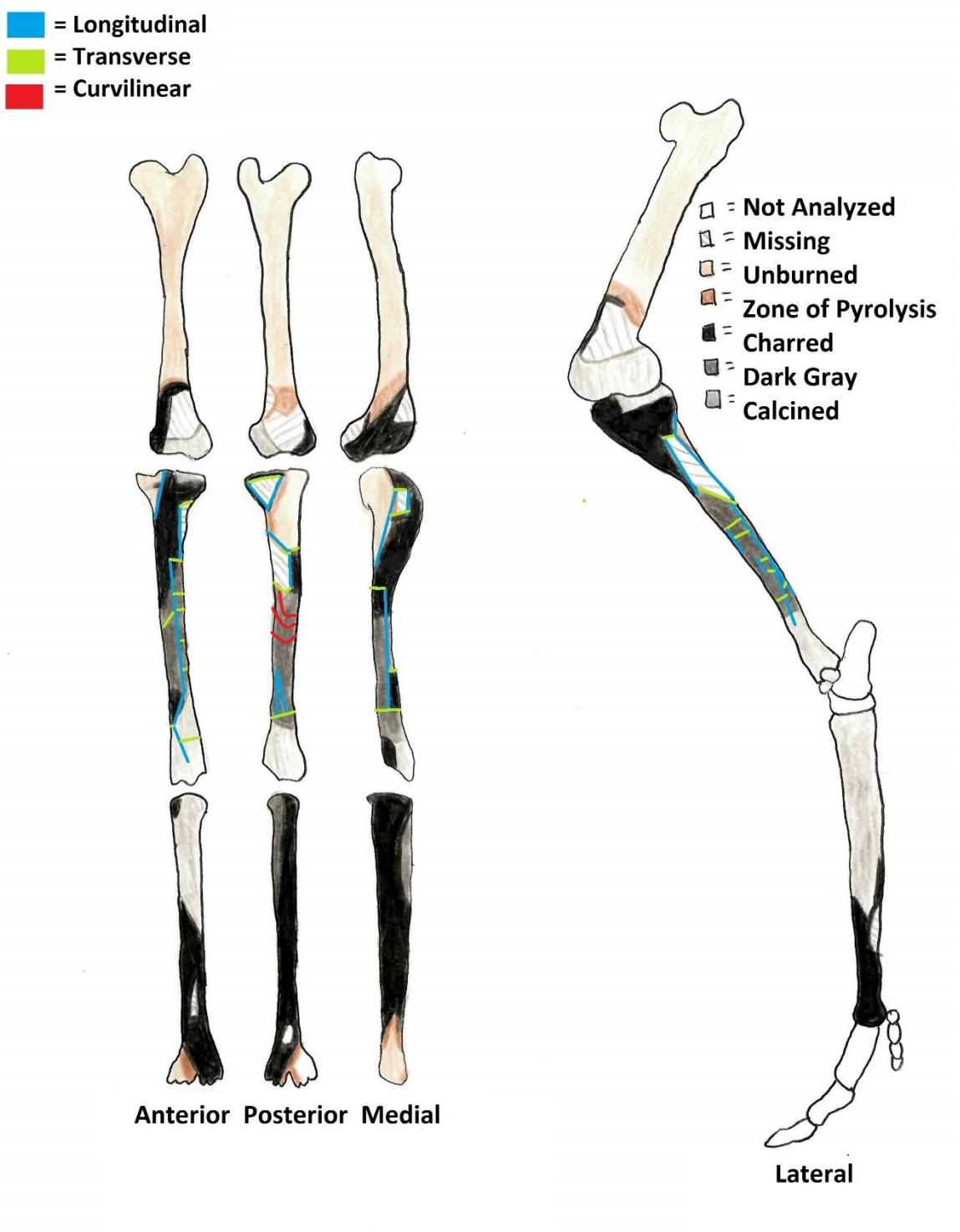

Figure 4.22. Diagram depicting the degree of burning of 2020-3 Left Hindlimb.

Figure 4.23. 2020-3 lateral view of the left tibia with shallow curvilinear fractures indicated by red arrows. The proximal end is on the top of the picture. The green arrow indicates the direction that the bone was burned.

After 20 minutes, the muscles of the shoulders were seen contracting dorsally, causing the shoulder to visibly flatten. After 40 minutes, both limbs were seen curling cranially, and after 20 minutes, they had curled all the way in to touch the shoulders. For the remainder of the burn, there was no observable movement of the muscles in either the shoulder or limb.

The bones of the left limb were variably burned (Table 4.1, Table 4.2, Figure 4.24). The humerus was completely unburned, and what was present of the ulna was mostly unburned, barring slight charring at the edge of the present proximal half. The metacarpal and radius were both mostly charred, but both showed many patterns of burning. Proximally the radius was unburned and distally the metacarpal was primarily unburned. Both were slightly fragmented with a few longitudinal and transverse fractures on each. On the distal metacarpal in the zone of pyrolysis, both delamination and a curvilinear fracture was observed (Table 4.3, Table 4.7). The curvilinear fracture was on the curved medial edge of the distal shaft and was concave distally (Figure 4.25). No muscles attach in the location the fracture falls and no other fractures connect with the curvilinear fracture (May, 1970).

Similar to the left limb, the humerus remained almost completely unburned, barring slight charring on the distal end (Table 4.1, Table 4.2, Figure 4.26). The remaining three bones of the right limb were more extensively burned than their counterparts in the left limb. The ulna was primarily charred and was missing the distal half. There were several shallow longitudinal and transverse fractures along the shaft. On the flat medial surface of the proximal end on the border between the zone of pyrolysis and the charred bone was a curvilinear fracture (Table 4.3, Table 4.7). This fracture was concave distally (Figure 4.27). Several muscles attach on the medial surface of the olecranon: triceps brachii, tensor fasciae antibrachii, and flexor carpi ulnaris (May, 1970) (Figure 3.1). A longitudinal fracture that starts superior to the set of curvilinear fractures terminates on the first fracture of the set. The radius exhibited slightly more extensive burning with dark gray being the major color pattern present. Many longitudinal and

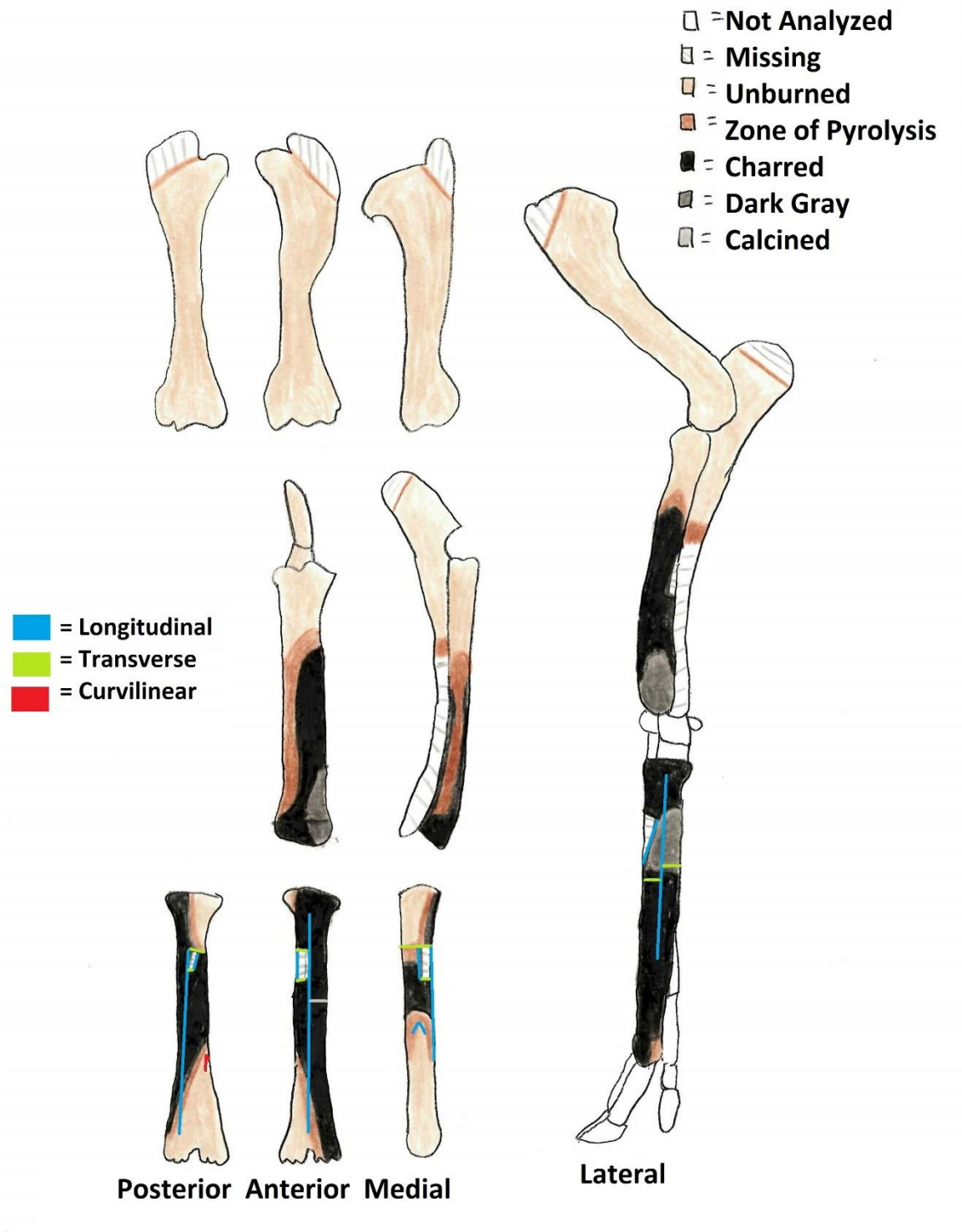

Figure 4.24. Diagram depicting the degree of burning of 2020-4 Left Forelimb.

Table 4.7. Fourth of bone, color score, uniformity score, and bone surface shape for all the curvilinear fractures of 2020-4.

Specimen	Limb pair	Side/Element	Location	1/4 of bone	Color Score	Uniformity Score	Bone Surface
2020-4	Fore	Left/Metacarpal	Medial Distal shaft	3	3	3	curved
2020-4	Fore	Right/Metacarpal	Distal Posterior shaft	4	1	3	flat
2020-4	Fore	Right/Radius	Posterior Proximal shaft	1	3	2	flat
2020-4	Fore	Right/Ulna	Medial Proximal end	1	3	4	flat
2020-4	Hind	Left/Metatarsal	Medial Proximal end	1	6	3	flat
2020-4	Hind	Left/Tibia	Posterior Lateral shaft	2	3	3	curved
2020-4	Hind	Left/Tibia	Anterior midshaft	2	3	3	curved

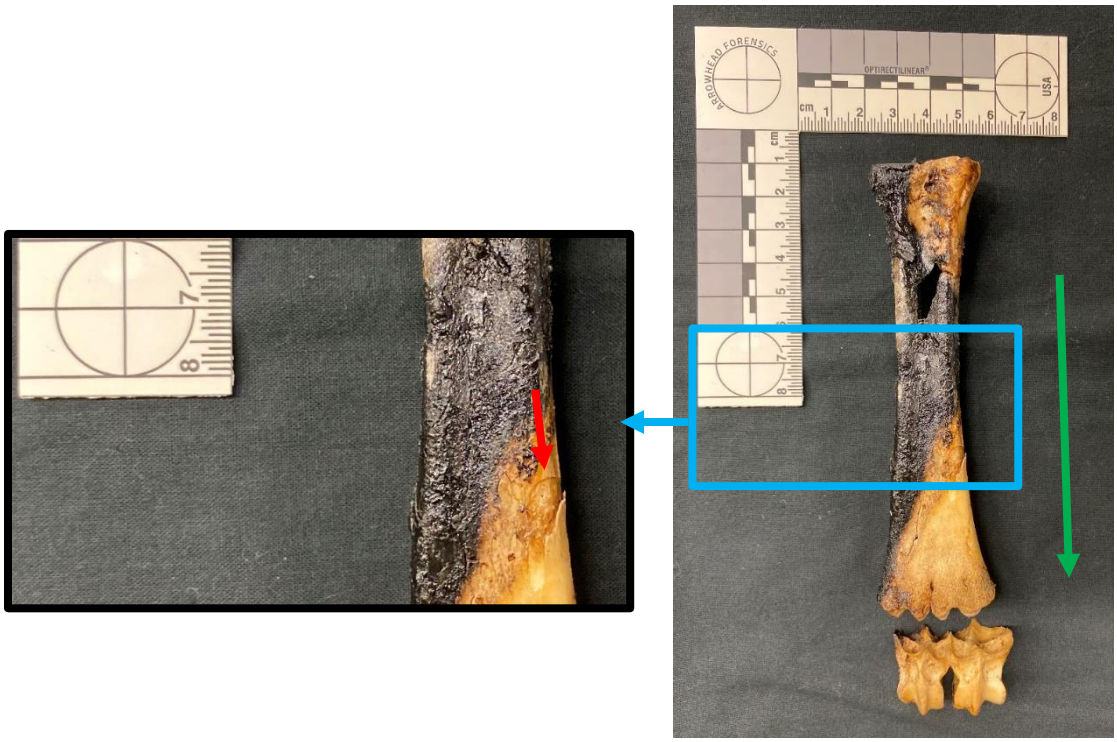

Figure 4.25. 2020-4 posterior view of the left metacarpal with a single curvilinear fracture in the zone of pyrolysis, up close image of curvilinear fractures indicated by a red arrow. The proximal end of the bone is at the top of the picture. The green arrow indicates the direction that the bone was burned.

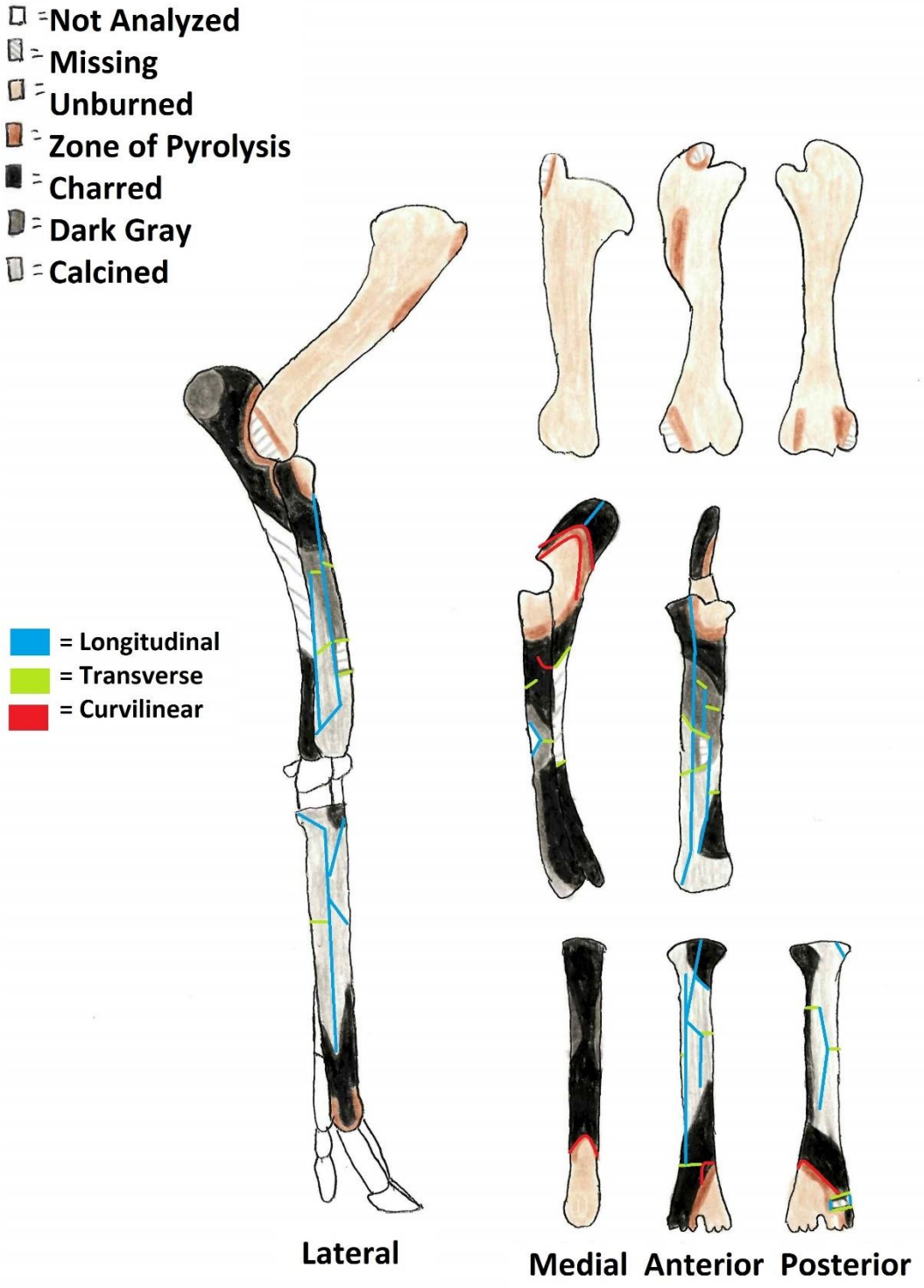

Figure 4.26. Diagram depicting the degree of burning of 2020-4 Right Forelimb.

Figure 4.27. 2020-4 medial view of the right ulna with shallow curvilinear fractures in the zone of pyrolysis. The proximal end of the bone is at the top of the picture. Red arrows indicate each fracture. The green arrow indicates the direction that the bone was burned.

transverse fractures come together making the radius highly fragmented. On the flat posterior side of the proximal shaft was a single shallow curvilinear fracture in the charred bone at the edge of the zone of pyrolysis that was concave proximally (Figure 4.28, Table 4.3, Table 4.7). The muscles that attach where this fracture falls are the same as all the previous radii. The fracture terminates into a neighboring longitudinal fracture. The metacarpal was mostly calcined with slight charring and an unburned medial distal end. There was slight fragmentation made up of a few longitudinal and transverse fractures. In the zone of pyrolysis on the flat posterior edge of the distal shaft was a single curvilinear fracture (Table 4.3, Table 4.7). No muscles attach to the part of the bone where the fracture fell (May, 1970) (Figure 3.1). The curvilinear fractures terminate into a small transverse fracture. Unlike the curvilinear fractures on the other two bones of this limb, the curvilinear fracture on the metacarpal was concave distally.

Specimen 2020-4 Hindlimbs

The ambient temperature at the beginning of the burn was 33°F with high humidity and winds. Both the night before and the morning of the burn, a mix of rain and snow occurred in Morgan County, where the burn site is located. This inclement weather made the ground, burn structure, and wood damp and slightly cold. The duration of the burn was 200 minutes. Both limbs began to slightly extend after 20 minutes. The left limb began to shift slightly laterally, and the right limb followed after. Both limbs continued to move laterally, and the muscles of the hips began to contract dorsally causing the haunch to visibly flatten out. After 96 minutes, the left limb began to move cranially until it was curled completely inward. The right limb continued to extend before it began its curl inward after 120 minutes. The muscles of the hips continued to contract dorsally, which shifted both limbs laterally. The left limb fractured, and calcined bone was visible. By the end of the burn, the right limb had shifted further laterally and only slightly inward, otherwise, there was no observable movement of the muscles or further burning of the limb.

Figure 4.28. 2020-4 posterior view of the right radius with single curvilinear fracture at the edge of the zone of pyrolysis, up close image of curvilinear fractures with red arrows to indicate the fracture. The proximal end of the bone is at the top of the picture. The green arrow indicates the direction that the bone was burned.

Unsurprisingly, the right limb was almost entirely unburned, besides slight charring and slight fragmentation of the distal tibia (Table 4.1, Table 4.2, Figure 4.29). The femur and metatarsal were both entirely unburned. The left limb was more extensively burned, though the femur was mostly unburned with charring on the distal end (Table 4.1, Table 4.2, Figure 4.30). The metatarsal was calcined proximally, and the majority of the shaft was dark gray with the distal end remaining unburned. Several longitudinal and transverse fractures were present. On the curved medial edge of the proximal end were several shallow concentric curvilinear fractures that were concave proximally (Table 4.3, Table 4.7, Figure 4.31). Several tendons attach to the medial proximal end of sheep metatarsals (May, 1970) (Figure 3.1). A longitudinal fracture on the posterior proximal end terminated into the first curvilinear fracture of the set. The tibia had low uniformity and was unburned proximally, charred for the majority of the shaft, and calcined distally. The shaft as highly fragmented, particularly the posterior, and had several transverse and longitudinal fractures. On the curved posterior lateral surface of the midshaft, there was a tiny set of shallow concentric curvilinear fractures (Table 4.3, Table 4.7). No muscle attach at the location where the curvilinear fractures fell (May, 1970) (Figure 3.1). These fractures were concave proximally and all terminated into a longitudinal fracture (Figure 4.32). On the anterior surface of the same tibia on the border of the charred bone and the zone of pyrolysis was the first of a set of two concentric curvilinear fractures (Table 4.3). This set of curvilinear fractures were also concave proximally and all terminate into a longitudinal fracture (Figure 4.33, Table 4.7). Several muscles attach to the curved anterior surface of the tibia: tibialis cranialis, semitendinosus, tensor fasciae latae, and biceps femoris (May, 1970) (Figure 3.1).

Statistical Analysis

Of the 56 long bones that make up the 16 limbs of the sample, 17 bones, or 30.4% of the total sample, exhibit curvilinear fractures (Table 4.8). Of the curvilinear fractures present, 14 of the fractures, or 77.8% of the total curvilinear fractures, are convex distally, which

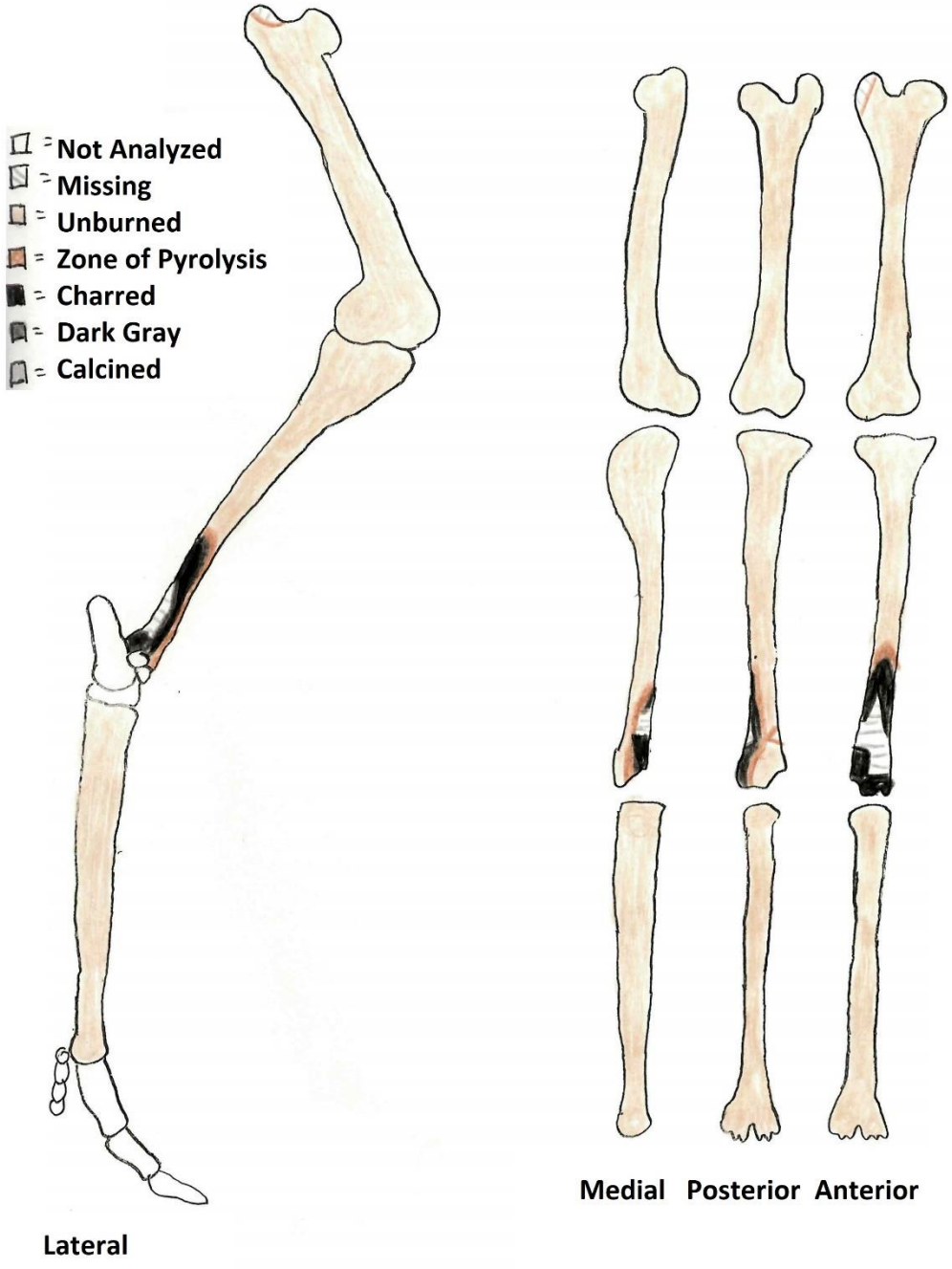

Figure 4.29. Diagram depicting the degree of burning of 2020-4 Right Hindlimb.

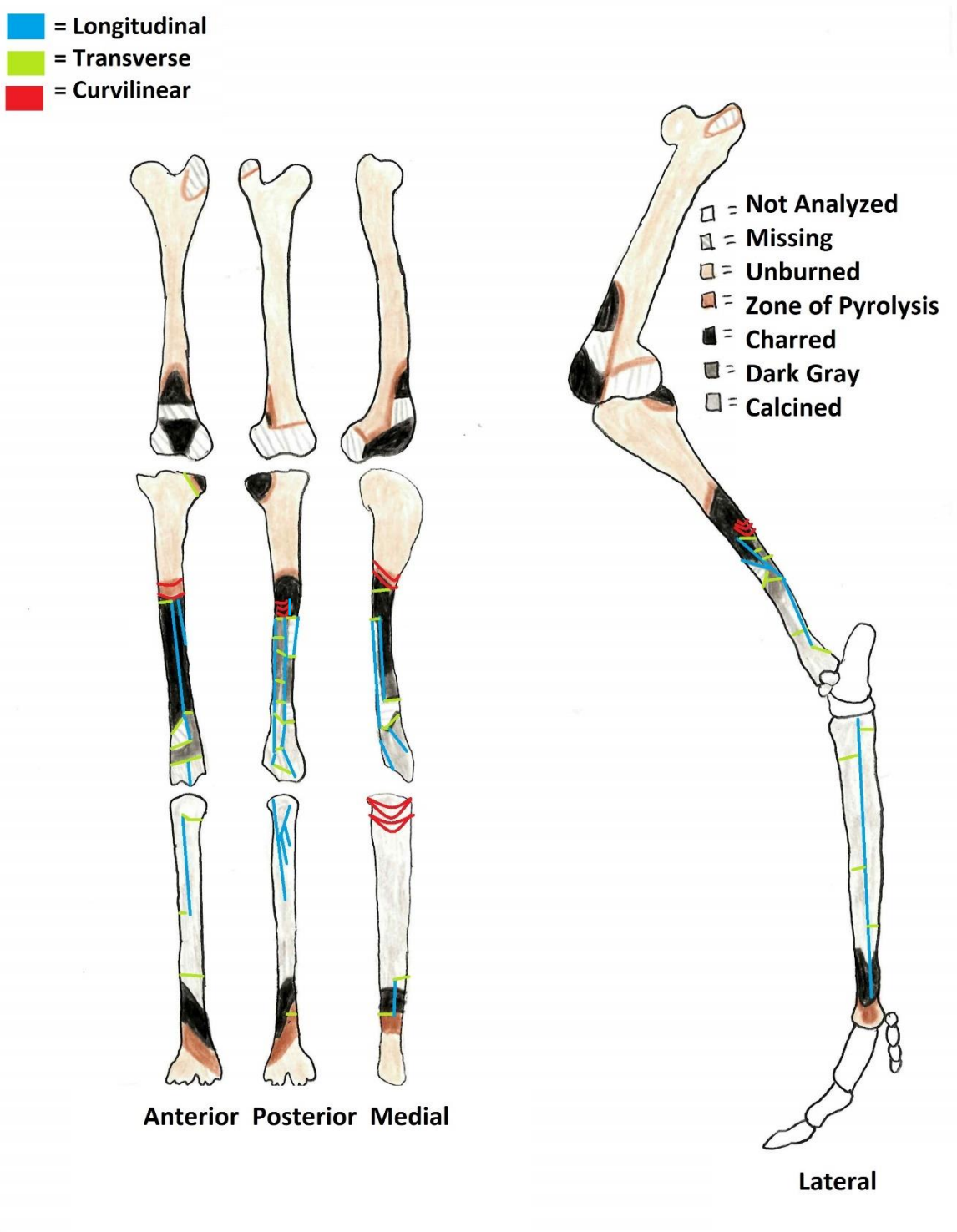

Figure 4.30. Diagram depicting the degree of burning of 2020-4 Left Hindlimb.

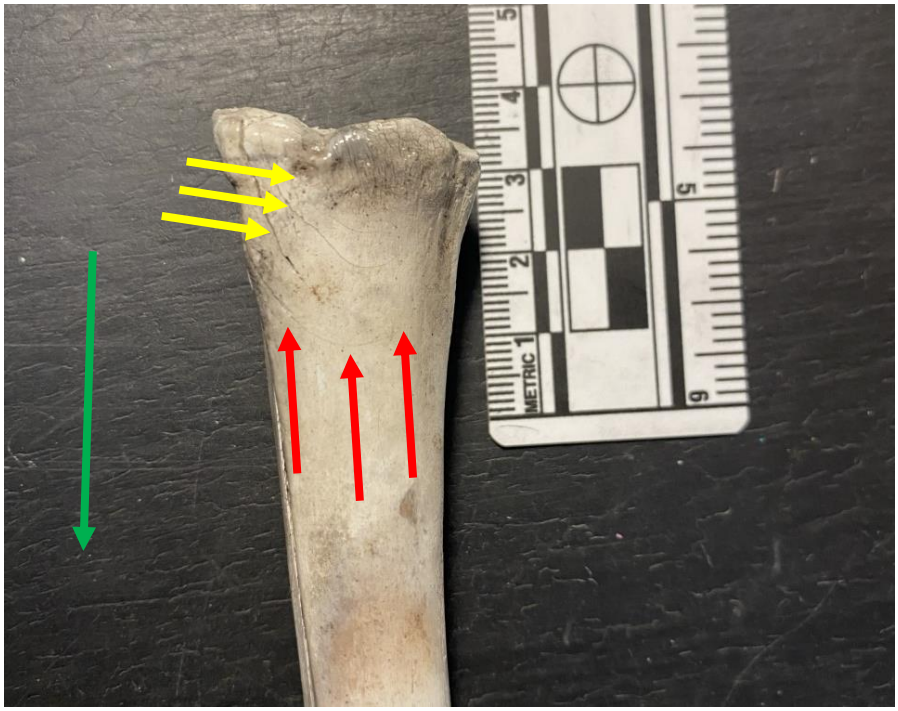

Figure 4.31. 2020-4 medial view of the left metatarsal with a set of shallow concentric curvilinear fractures. The proximal end is at the top of the photo. The red arrows indicate the first curvilinear fracture in the set and the yellow arrows indicate the subsequent fractures. The green arrow indicates the direction that the bone was burned.

Figure 4.32. 2020-4 lateral view of the left tibia with a set of shallow concentric curvilinear fractures. The proximal end of the bone is on the top of the picture. Red arrows indicate the first and last of the shallow concentric curvilinear fractures. The green arrow indicates the direction that the bone was burned.

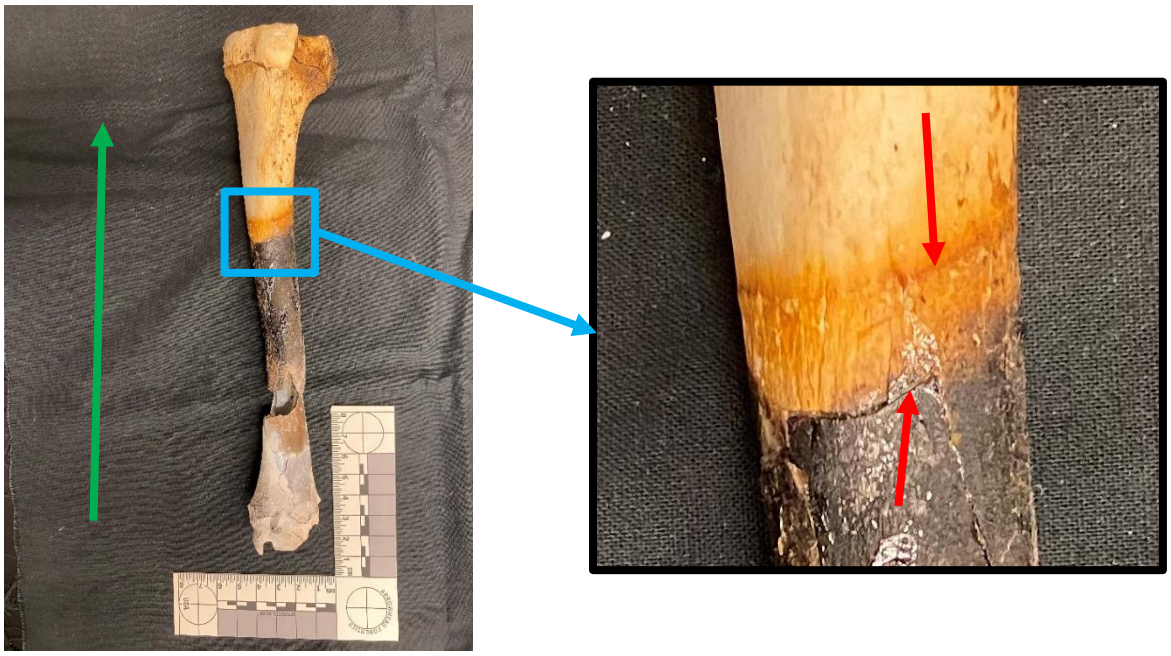

Figure 4.33. 2020-4 anterior view of the left tibia, up close image of curvilinear fractures. The proximal end of the bone is at the top of the picture. With a red arrow indicating each fracture. The green arrow indicates the direction that the bone was burned.

Table 4.8. Crosstabulation of curvilinear fracture convexity for total sample.

			Convexity Direction			
			Convex Proximally	Convex Distally	Not Applicable	Total
Curvilinear Fractures	Absent	Count	0	0	39	39
		% of Total	0.0%	0.0%	69.6%	69.6%
	Present	Count	4	13	0	17
		% of Total	7.1%	23.2%	0.0%	30.4%
Total		Count	4	13	39	56
		% of Total	7.1%	23.2%	69.6%	100.0%

was the predicted direction based on the sample's position relative to the fire during burning (Table 4.8, Table 4.9). Four of the curvilinear fractures were convex proximally this means that of the curvilinear fractures present, 22.2% had a convexity opposite to the predicted direction (Table 4.8, Table 4.9). Specimen 2020-1 Fore had three bones with curvilinear fractures, the radius and the ulna of the left limb and the radius of the right limb (Table 4.3). All of the curvilinear fractures seen in 2020-1 Fore were convex distally, encompassing 5.4% of the overall specimens and 17.6% of the bones with curvilinear fractures (Table 4.8, Table 4.10, Table 4.11). No curvilinear fractures were observed in 2020-1 Hind.

Specimen 2020-2 Fore had four bones with curvilinear fractures; left radius, left ulna, right radius, right metacarpal (Table 4.3). The curvilinear fractures on three of these four bones from the specimen were convex distally. Only the right metacarpal had curvilinear fractures that were convex proximally. 2020-2 Hind had two bones with curvilinear fractures, the left and right tibia (Table 4.3). The curvilinear fractures on both of these bones were convex distally. The curvilinear fractures of both 2002-2 Hind and 2020-2 Fore made up 10.7% of the total bones, 8.9% of which are convex distally and 1.9% that were convex proximally (Table 4.10, Table 4.11).

Specimen 2020-3 Fore and Specimen 2020-3 Hind each only had one bone with observable curvilinear fractures, the right radius and left tibia respectively (Table 4.3). For both of these, the curvilinear fractures were convex distally. Overall, the curvilinear fractures of this specimen made up 3.6% of the total bones (Table 4.10, Table 4.11). Specimen 2020-4 Fore had four bones with curvilinear fractures: left metacarpal, right metacarpal, right radius, and right ulna (Table 4.3). Only the curvilinear fractures on the right radius were convex distally; the fractures of the three other bones were convex proximally. Of the curvilinear fractures, four were convex proximally, three of the four within this specimen (Table 4.10, Table 4.11). 2020-4 Hind limb had two bones with curvilinear fractures, the left tibia and left metatarsal. The curvilinear fractures on both of

Table 4.9. Crosstabulation of curvilinear fractures and directionality.

			Convexity Direction		
			Convex Proximally	Convex Distally	Total
Curvilinear Fracture	Curvilinear Fracture	Count	4	14	18
		% of Total	22.2%	77.8%	100.0%

Table 4.10. Crosstabulation of curvilinear fracture presence and absence by specimen.

			Curvilinear Fractures		
			Absent	Present	Total
Specimen	2020-1	Count	11	3	14
		% of Total	19.6%	5.4%	25.0%
	2020-2	Count	8	6	14
		% of Total	14.3%	10.7%	25.0%
	2020-3	Count	12	2	14
		% of Total	21.4%	3.6%	25.0%
	2020-4	Count	8	6	14
		% of Total	14.3%	10.7%	25.0%
Total		Count	39	17	56
		% of Total	69.6%	30.4%	100.0%

Table 4.11. Crosstabulation of curvilinear fracture convexity by specimen.

			Convexity Direction			
			Convex Proximally	Convex Distally	Not Applicable	Total
Specimen	2020-1	Count	0	3	11	14
		% of Total	0.0%	5.4%	19.6%	25.0%
	2020-2	Count	1	5	8	14
		% of Total	1.8%	8.9%	14.3%	25.0%
	2020-3	Count	0	2	12	14
		% of Total	0.0%	3.6%	21.4%	25.0%
	2020-4	Count	3	3	8	14
		% of Total	5.4%	5.4%	14.3%	25.0%
Total		Count	4	13	39	56
		% of Total	7.1%	23.2%	69.6%	100.0%

these bones were convex distally. Overall, the curvilinear fractures found in both of these specimens total 10.7% of the total bones, 5.4% convex proximally and 5.4% convex distally (Table 4.10, Table 4.11).

The color and uniformity scores for the fourth of the bone on which the curvilinear fractures fell and whether the bone surface was curved or flat was noted in Tables 4.4, 4.5, 4.6, and 4.7. Twelve or 66.7% of the curvilinear fractures recorded fell within an area that was primarily charred (Table 4.12, Figure 3.34). The next highest was gray with three or 16.7%. The remaining three color scores, calcined, light gray, and brown all had one, or 5.6%, fracture fall in a fourth scored with the color (Table 4.12, Figure 3.34). Nine or 50% of the curvilinear fractures recorded fell within an area with three patterns of burning (Table 4.13, Figure 3.35). Four patterns of burning were the next highest with 5 instances of 27.8%, followed by two patterns of burning with two instances at 11.1% (Table 4.13, Figure 3.35). The remaining two patterns of burning, uniform and five patterns of burning, each had one instance at 5.6% (Table 4.13, Figure 3.35). Eleven or 61.1% of the fractures fell on a bone surface that was flat and seven or 38.9% fell on a curved bone surface (Table 4.14, Figure 3.36).

An *A posteriori* power analysis was conducted to identify possible samples sizes at varying levels of effect size and power (Table 4.15). The smallest sample size possible while still maintaining a significance level of 0.05 is 12, with an effect size of 0.5 and statistical power at 0.4. The largest possible sample size is 490, with an effect size of 0.1 and statistical power at 0.6. For a repetition of this study to have a high effect size (0.5) and high statistical power (0.8), a sample size of 32 is needed. While the sample size of this study was not large enough to provide a statistically significant relationship between the convexity of curvilinear fractures and the position of the body relative to the fire, it does allow for a discussion on how the observations of this study relate to the previous literature on the subject. This study also provides a model for future exploration of the topic.

Table 4.12. Crosstabulation of color score and curvilinear fracture direction.

			Color Score					
			Brown	Charred	Gray	Light Gray	Calcined	Total
Convexity Direction	Convex Proximally	Count	1	3	0	0	0	4
		% of Total	5.6%	16.7%	0.0%	0.0%	0.0%	22.2%
	Convex Distally	Count	0	9	3	1	1	14
		% of Total	0.0%	50.0%	16.7%	5.6%	5.6%	77.8%
Total		Count	1	12	3	1	1	18
		% of Total	5.6%	66.7%	16.7%	5.6%	5.6%	100.0%

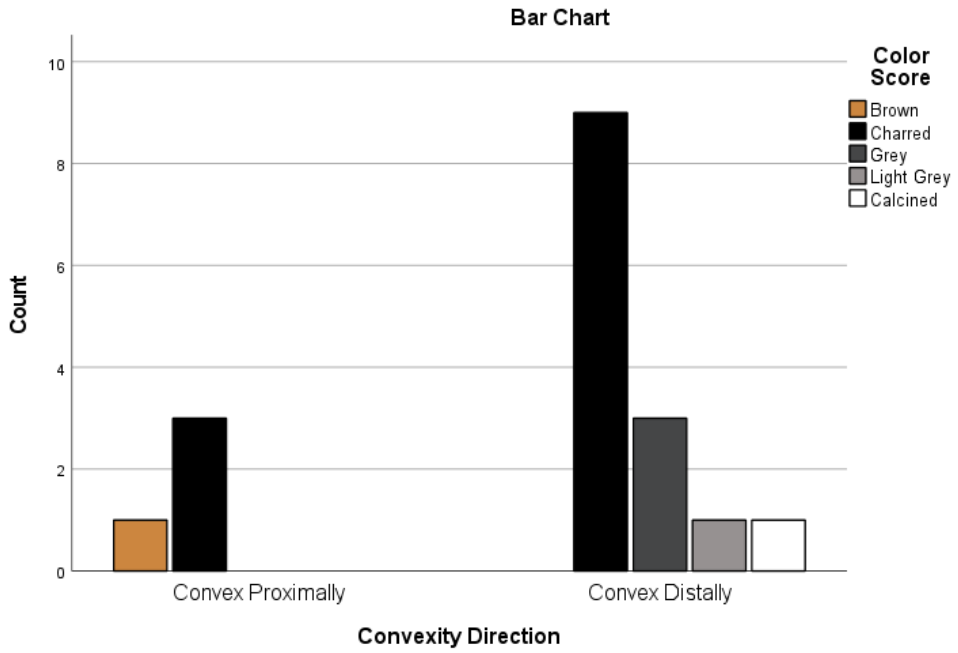

Figure 4.34. Bar chart depicting the count for curvilinear fractures convex proximally or distally by primary color of burn pattern.

Table 4.13. Crosstabulation of uniformity score and curvilinear fracture direction.

			Uniformity Score					
			Uniform	Two Patterns of Burning	Three Patterns of Burning	Four Patterns of Burning	Five Patterns of Burning	Total
Convexity Direction	Convex Proximally	Count	0	0	3	1	0	4
		% of Total	0.0%	0.0%	16.7%	5.6%	0.0%	22.2%
	Convex Distally	Count	1	2	6	4	1	14
		% of Total	5.6%	11.1%	33.3%	22.2%	5.6%	77.8%
Total		Count	1	2	9	5	1	18
		% of Total	5.6%	11.1%	50.0%	27.8%	5.6%	100.0%

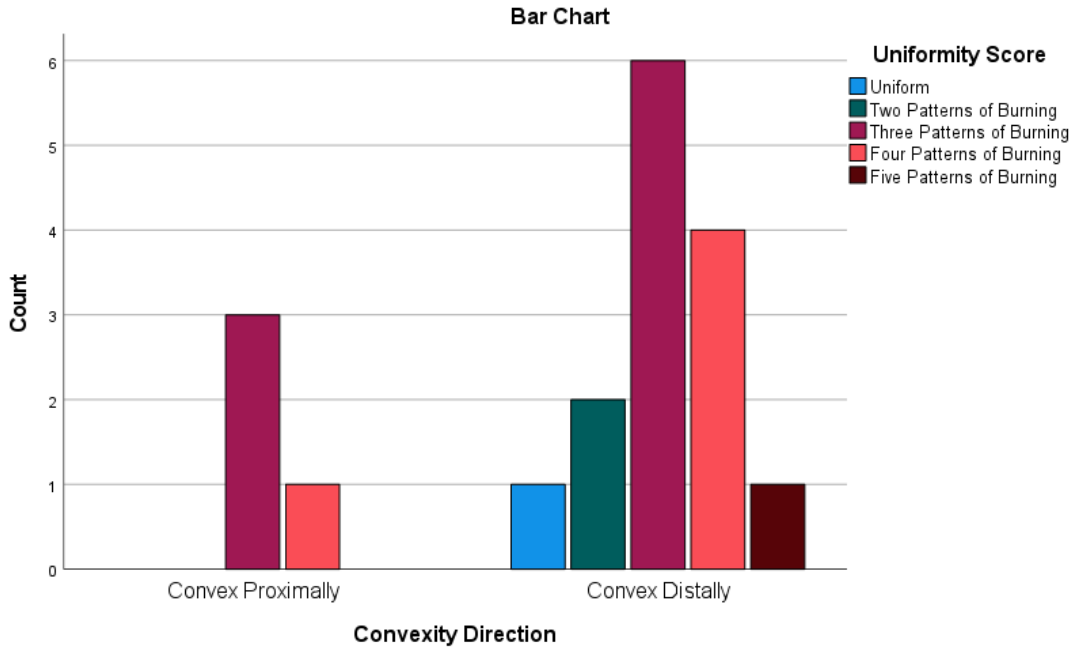

Figure 4.35. Bar chart depicting the count for curvilinear fractures convex proximally or distally by uniformity of burn pattern.

Table 4.14. Crosstabulation of bone surface and curvilinear fracture direction

			Bone Surface		
			Flat	Curved	Total
Convexity Direction	Convex Proximally	Count	3	1	4
		% of Total	16.7%	5.6%	22.2%
	Convex Distally	Count	8	6	14
		% of Total	44.4%	33.3%	77.8%
Total		Count	11	7	18
		% of Total	61.1%	38.9%	100.0%

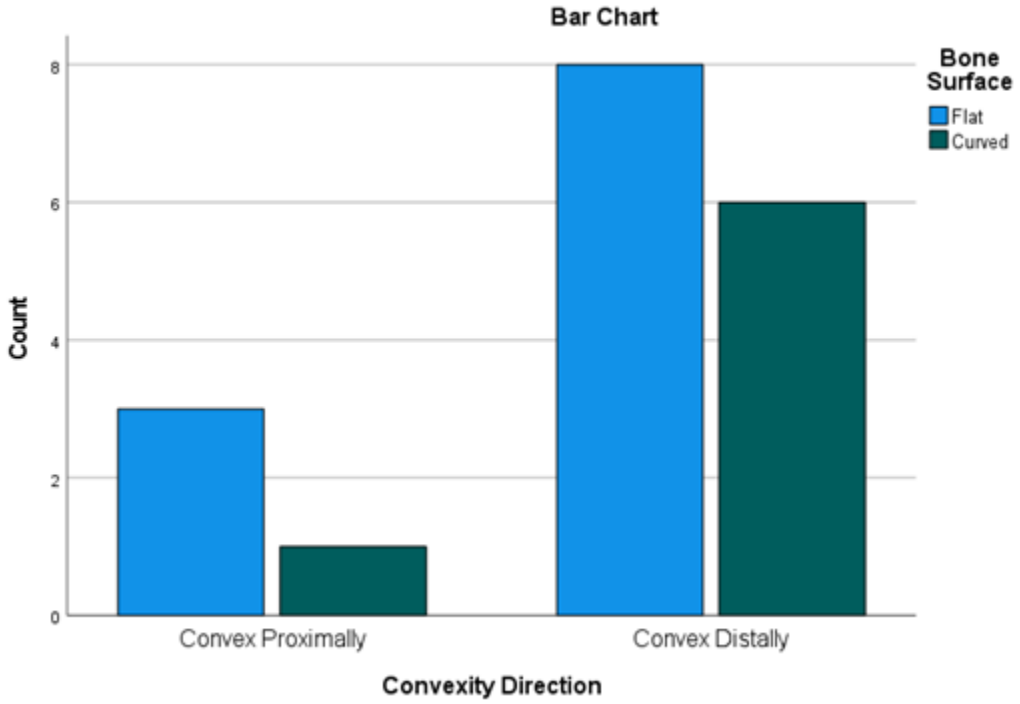

Figure 4.36. Bar chart depicting the count for curvilinear fractures convex proximally or distally by if the bone surface where the curvilinear fracture fell was flat or curved.

Table 4.15. Results of an *a posteriori* power analysis to find the needed sample size at varying effect sizes and with varying statistical power.

Effect Size (W)	Sample Size (N)	Degrees of Freedom (df)	Sig. Level	Power
0.5	31.3954	1	0.05	0.8
0.3	87.2095	1	0.05	0.8
0.1	784.886	1	0.05	0.8
0.5	19.5943	1	0.05	0.6
0.3	54.4286	1	0.05	0.6
0.1	489.857	1	0.05	0.6
0.5	11.6458	1	0.05	0.4
0.3	32.3495	1	0.05	0.4
0.1	291.145	1	0.05	0.4

CHAPTER FIVE
DISCUSSION AND CONCLUSION

Observation Notes and Video Recordings

One of the ways curvilinear fractures are thought to be created is through muscles shrinking and pulling on the periosteum, leading to fractures on the underlying bone (Pope, 2007; Symes et al., 2008; Williams, 2020). As a body without modification or trauma burns, it moves in a predictable manner as the muscles shrink, pulling the body into the pugilistic pose (Pope, 2007; Symes et al., 2008; Williams, 2020). For the sheep to be a good analog for curvilinear fractures in human bone, the muscles of the sheep would need to shrink and pull on the bones similar to how they shrink and pull on human bone. The sample of sheep limbs in this study have several possible factors that may impact their use as a model for curvilinear fractures in humans. One such factor is the disarticulation of the limbs. While the disarticulation of the limb from the body may impact how the muscles shrink, care was taken to ensure that all major muscles that insert into the long bones of each limb remained intact.

Another factor that may have influenced how the limbs move as the muscles shrink is the difference between the anatomy of sheep and humans. It was previously discussed how the microstructure of sheep bones and their muscle to fat ratio made them ideal for previous studies as a nonhuman model, but other differences may impact their use as a model (Thompson et al., 2011; Thompson and Chudek, 2007; Shipman et al., 1984; Macoveciuc et al., 2017; Dempsey et al., 2018; Thompson, 2005; Carroll and Smith, 2018). While both species are mammals and have many musculoskeletal similarities, the differences may impact the pattern of movement during burning. The most glaring difference is the locomotion pattern. Sheep are quadrupedal while humans are bipedal, which causes a difference in body proportion and position. Another big difference is that sheep have a singular metacarpal and metatarsal, classified as metapodials. Metapodials are found in ungulate animals and make up the distal portion of the limb (May, 1970).

Metapodials are considered long bones, unlike the metacarpals and metatarsals of humans which are classified as short bones.

There is also a difference in terminology when referring to the joints of the limbs (Figure 5.1). The fetlock joint is the articulation between the phalanx and metacarpal or metatarsal (May, 1970). The joint between the radius and the carpals is referred to as the knee in sheep and hock is used to refer to the joint between the tibia and tarsals (May, 1970). The hinge joint between the radius, ulna, and humerus is also called the elbow, but the synovial joint between the tibia and femur is called the stifle in sheep (May 1970). Through the observation notes taken during the burns and review of the videos of each burn, the observable movement of the limbs of the sample can be compared to the predictable patterns documented in the literature.

The majority of the limbs were seen moving consistently during burning, barring a few outliers. The observed pattern of muscle shrinkage based on this sample is as follows: limbs extend and straighten out, they then curl cranially first at the fetlock, then the knee and hock, then finally at the elbow and stifle. For the forelimb, the final position was very similar to the “boxer’s pose” of the human pugilistic pose with the hoof near or touching the muscles of the shoulder (Figure 4.1). The end position of the hindlimb was also similar to the human pugilistic pose, with the fetlock almost resting against the hock and the slight flexion of the stifle and hip.

In a few forelimb and hindlimb specimens, the distal portion of the limb fractured and detached prior to the limb curling all the way cranially. The fracture occurred primarily in the tibiae, radii, and ulnae, though some were observed at or below the hock or knee. In these instances, the end position was altered, but movement was often still observed in the remaining portion of the limb still attached to the shoulder or rump.

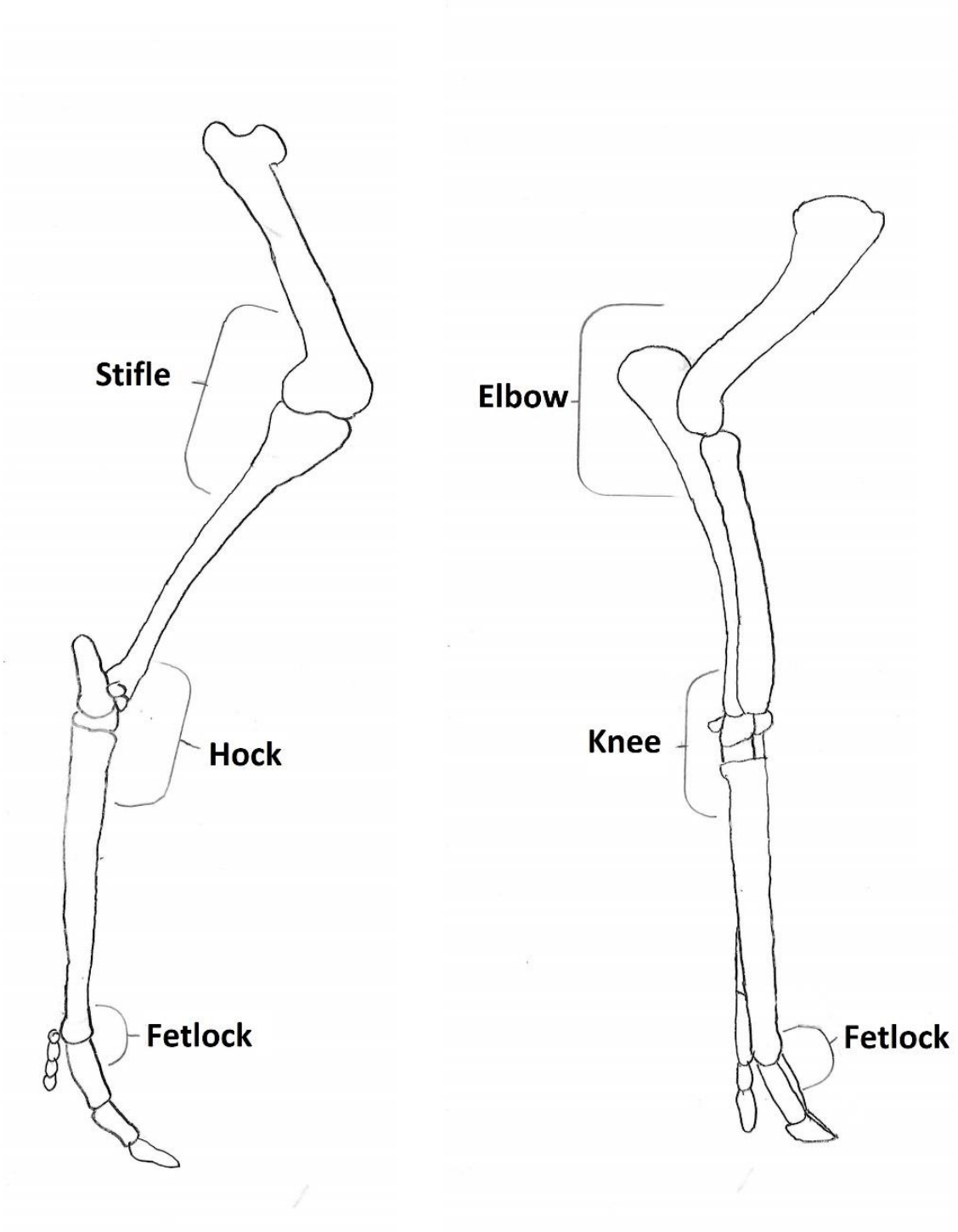

Figure 5.1. Diagram showing the appropriate anatomical terms for the limb joints of sheep. On the left is the hindlimb and the right is the forelimb.

One outlier was the right hind limb of 2020-1 (Figure 5.2). During the burn, the limb was seen extending towards the beginning of the burn, but then very little movement was observed until the very end of the burn. As the tissue around the tibia shaft burned away, the limb was seen curling cranially at the fetlock and hock before it stopped progressing cranially and instead shifted medially. Due to high winds on the day this specimen was burned, maintaining the fire was challenging, particularly on the right side. The right side of the burn structure housed the openings for feeding fuel into the fire but also left it exposed to the wind.

Despite a few outliers and differences, the muscles of the disarticulated sheep limbs moved in a similar pattern and resulted in a similar end position to the pugilistic pose. If curvilinear fractures are caused by kinetic energy generated by muscle shrinkage, then sheep having a similar pattern of muscle shrinkage and tissue destruction makes them a good analog for how human remains burn and how curvilinear fractures are created.

Curvilinear Fractures by Skeletal Elements

One way to examine the curvilinear fractures in the sample is to discuss them by skeletal element. Looking at the extent of burning across the total sample of each skeletal element and looking at where the fracture(s) fall in relation to the burn pattern could provide insight into where and why curvilinear fractures appear. Of the 17 bones with observable curvilinear fractures, 12 were in the forelimb, with six of those being radii, making radii the element with the most curvilinear fractures.

There was very little burning observed on the humeri and femora. This lack of heat alteration was due to the thick layer of muscle and tissue surrounding them. When the burning ceased for all specimens, a majority of the hip and shoulder muscles remained intact. Across the eight specimens of humeri and femora, only slight burning to the

Figure 5.2. A series of images from the burning of 2020-1 Hind highlighting the movement of the right limb as it burned.

proximal and distal ends was observed. The burning observed on the right humerus of 2020-2 was quite extensive but was only on the anterior and lateral surfaces. With the minimal burning seen to the proximal bones of each limb, it was not surprising that no curvilinear fractures were observed on the femora and humeri.

Of the metapodials, metacarpals and metatarsals, four of the 16 remained completely unburned. Thirteen had observable burning, though the left metacarpal of 2020-3 was mostly unburned with an observable zone of pyrolysis around missing portions of the anterior, posterior, and most of the lateral surface of the shaft. Of the remaining 12 with visible burning, only five had observable unburned portions all of which were on the distal end. Three metacarpals and one metatarsal had observable curvilinear fractures. The curvilinear fractures on the three metacarpals were convex proximally, and on the metatarsal, they were convex distally. The curvilinear fractures of all three metacarpals fell in or next to the zone of pyrolysis. Two fell on a flat bone surface and one on a curved edge. On the metatarsal, the curvilinear fractures were located on a completely calcined portion of the shaft that was flat.

For five of the eight tibiae, the proximal end remained unburned while the distal ends were burned. The extent of this burning varied from the distal end only being partially burned to burning up to a little above midshaft. One of the eight, 2020-1 right, was missing a good portion of the posterior shaft with slight charring and a zone of pyrolysis around the edge. The last two tibiae, both from 2020-3, had extensive burning, one covering the proximal end and one almost reaching the proximal end. The likely reason for this trend of unburned proximal ends seen in the majority of the tibiae was the thick muscles surrounding the hock. Four of the eight tibiae had curvilinear fractures, all of which were convex distally. The left tibia of 2020-4 had two observable instances of curvilinear fractures, one in the zone of pyrolysis and one in dark gray bone. One of the other tibia's curvilinear fractures fell in the zone of pyrolysis, and the fractures on the other two fell in dark gray or charred bone. All of the fractures found on the tibia were located on curved portions of the diaphysis.

Six of the radii have observable curvilinear fractures, and three of the paired ulnae also have observable curvilinear fractures. The eight radii were the most extensively burned element of the total sample. All but three of the eight had very little unburned bone present. The three with a higher amount of unburned bone were primarily only unburned on the most proximal fourth. Four of the six radii with observable curvilinear fractures had these fractures falling near or on the zone of pyrolysis. The fractures of the remaining two fall around midshaft in dark gray bone. Two of the curvilinear fractures on the ulnae fell around midshaft in dark gray bone, and the final one was within the zone of pyrolysis on the medial surface of the proximal end. The curvilinear fractures on all radii and two of the ulnae were convex distally. The ulna with the curvilinear fracture on the proximal end was the right ulna of 2020-4 and was the only one with a proximally convex curvilinear fracture. This ulna, combined with the three metacarpals with proximally convex curvilinear fractures, were the only four proximally convex fractures in the entire sample. All of the curvilinear fractures on the radii fell on the flat posterior surface of the diaphysis which houses several muscles that originate and insert on the interosseus ligament or the surrounding bone. The locations of the curvilinear fractures on the ulnae were variable in location and surface, but the two that fell along midshaft are impacted by the same muscles that attach to the posterior surface of the radii.

In total, there were 18 instances of curvilinear fractures on 17 out of the 56 bones that made up the sample. In this sample, the majority of the fractures fell within charred bone, but were seen in all but unburned bone. Similarly, the fractures primarily fell within an area with three patterns of burning but were seen in all five uniformity categories. Despite previous literature stating that curvilinear fractures primarily occur in remains that are calcined, within this sample they occurred in all patterns of burn color and uniformity barring unburned bone (Ellingham and Sandholzer, 2020; Shipman et al., 1984). Of note, all but one of the curvilinear fractures were concave in the direction of unburned bone. The shallow concentric curvilinear fractures on proximal end of the left metatarsal of 2020-4 were concave towards a completely calcined proximal end.

Curvilinear fractures are said to occur as heat moves along a bone and are convex in the direction of the heat, which would appear on the bone with the fractures being concave towards the unburned bone. For this sample, this observation was true in all but one instance.

Curvilinear Fractures Related to Other Factures

As previously mentioned, existing fractures can impact the ability of a bone to deal with stress and strain. The extent of fracturing to all of the bones with curvilinear fractures ranges from slight to highly fractured. In all but three instances, the curvilinear fractures of the sample interacted with other fractures. Eight of the curvilinear fractures had one or two fractures terminating into them. This means that the curvilinear fractures came first in these instances and the energy that formed the other fractures dissipated once they came into contact with the curvilinear fractures. Conversely, six of the curvilinear fractures terminate into other fractures meaning those other fractures came first. For the final of the 18 curvilinear fractures, it is both terminated into by a transverse fracture and it terminated into a longitudinal fracture. This means the transverse came prior to the curvilinear fracture and the curvilinear fracture came prior to the longitudinal fractures.

All of the bones with curvilinear fractures had several other fractures along the shaft, some only had a few and some had many. The chronology of all of the fractures was not recorded, but the fragmented nature of the burned bone would impact the bones ability to resist stress and strain. If those fractures came prior to the curvilinear fractures, like the seven fractures described above, then those bones would have been more susceptible to fracturing. It is possible that prior to the nine curvilinear fractures that have fractures terminating into them and the three curvilinear fractures that do not interact with any other fractures, could have come after other fractures on the bones. If that is the case, even if the fractures did not interact with the curvilinear fractures, they would still have impacted the structural integrity of the bone.

Curvilinear Fractures Related to Muscle Attachments

Of the 18 curvilinear fractures present, 13 were directly associated with muscle attachment sites. For the location of the curvilinear fractures on the posterior side of five of the radii, four muscles attach in the locations of the observed fractures. The first of these muscles is the biceps brachii which attaches on the rudimentary tuberosity and the interosseus ligament. This muscle works to flex the elbow, extend the shoulder, and tense the facia (May, 1970) (Figure 3.1). The next two muscles are the extensor digitorum lateralis and extensor digitorum comminus. Both muscles attach to the radius on the interosseus ligament and, like their name suggests, act on extending the carpus and digits as well as flexing the elbow (May, 1970) (Figure 3.1). The final muscle that attaches at the location of the curvilinear fractures on the radii is the brachialis, which attaches on the interosseus ligament and flexes the elbow (May, 1970) (Figure 3.1).

The curvilinear fracture on the left ulna of 2020-2 fell at the location of three muscle attachments. Two of these muscles were mentioned above, the biceps brachii and the extensor digitorum communis, which both attach to the interosseus ligament (May, 1970) (Figure 3.1). The remaining muscle that attaches to the medial midshaft of the ulna is the abductor pollicis longus. This muscle attaches to the proximal interosseus space on the ulna and extends and rotates the carpus (May, 1970) (Figure 3.1). The extensor digitorum communis also attaches at the location of the curvilinear fractures on the left radius and ulna of 2020-1. The proximally convex fracture on the proximal end of the right ulna of 2020-4 is the location of attachment for three muscles: triceps brachii, tensor fasciae antibrachii, and flexor carpi ulnaris. All three attach on various parts of the medial olecranon (May, 1970) (Figure 3.1). The triceps brachii extends the elbow and the tensor fasciae works to assist it while also tensing the fascia. The flexor carpi ulnaris muscle flexes the carpus and extends the elbow (May, 1970) (Figure 3.1). On the posterior distal end of the right metacarpal of 2020-2, the observed curvilinear fractures fall at the location of attachment for the flexor digitorum superficialis. This muscle works to extend both the carpus and digits while also flexing the elbow (May, 1970) (Figure 3.1).

The popliteus muscle attaches at the location of the curvilinear fractures on the posterior midshaft of the left tibia of 2020-3. This muscle flexes the stifle and rotates the tibia (May, 1970) (Figure 3.1). The final two curvilinear fractures that are located at sites of muscle attachment are on the right tibia of 2020-2 and left tibia of 2020-4. There are four muscles that attach at the location of these fractures: tibialis cranialis, semitendinosus, biceps femoris, and tensor fasciae latae. The first three muscles all attach to the tibia crest, but all perform different actions to move the limb (May, 1970) (Figure 3.1). The tibialis cranialis flexes the hock and the biceps femoris extends the hip, stifle, and hock. The semitendinosus extends the hip and fetlock, flexes the stifle, and acts to rotate the distal limb (May, 1970) (Figure 3.1). The final muscle does not directly attach to the tibia, but instead attaches to the fascia which attaches at the tibial crest. This muscle works to flex the hip, extend the stifle, and tense the fascia (May, 1970) (Figure 3.1). While several curvilinear fractures were associated with sites of muscle attachment, there were five that were not. Which, if kinetic energy generated by shrinking muscles is the cause for curvilinear fracture formation like the literature suggests, it would make sense for curvilinear fractures to be located at sites of muscle attachment (Pope, 2007; Symes et al., 2008; Williams, 2020). Based on the observations from this study that was not always the case.

Observations Related to Existing Literature

The literature discusses how the convexity of a curvilinear fractures relates to how the heat moved along a bone as the tissue shrinks and burns (Pope, 2007; Symes et al., 2008; Williams, 2020). More specifically, it is suggested that the convexity of the fracture points in the direction of the fire (Pope, 2007). Research states that the convexity of curvilinear fractures can be used as clues to how a body burned in an instance of high calcination and fragmentation (Pope, 2007). Based on the observations above, it seems to

be true that curvilinear fracture convexity can be used to indicate how fire consumed a bone, but not necessarily the body's position relative to the heat source.

While the majority of the curvilinear fractures present in the sample were convex distally, which was the anticipated direction based on the origin of the fires and position of the bodies, this was likely related more to the pattern of tissue destruction. In all but one instance, the curvilinear fractures were concave in the direction of unburned bone. This suggests that they are created as tissue is progressively destroyed and the bone is exposed to the heat. Looking at the four bones with curvilinear fractures that were convex proximally, three of the four were metacarpals with a burn pattern indicating the proximal end of the bone was the first to be consumed. The fracture convexity was not pointing towards the source of heat, but rather the direction in which the tissue surrounding the bone was consumed.

The fourth bone with a proximally convex curvilinear fracture was an ulna. When looking at the burn pattern both on the ulna and on the neighboring radius and metacarpal, it seemed that the bones were burned starting at the lateral knee (Figure 4.27). The medial shaft of all three bones were primarily charred, while the lateral shaft of the radius and metacarpal were calcined. The medial portions of the radius and ulna that articulate with the humerus remain unburned. The charring on the olecranon of the ulna suggests that the lateral portion was exposed to the heat first, and then the heat moved over the proximal end and around the posterior edge to begin consuming the medial surface of the bone. The curvilinear fractures reflect this pattern of tissue destruction.

While the observations in the study seem to align with the literature about the relationship between fracture convexity and how heat moves along the bone as it burns, there is one outlier that does not reflect this pattern. For this outlier, the left metatarsal from 2020-4, a set of shallow concentric curvilinear fractures were seen on the medial surface of the proximal shaft. Unlike all the other fractures in the sample, this set was concave in the

direction of calcined bone. Looking at the overall burn pattern of the metatarsal and the neighboring tibia, the pattern indicated the burning began at the hock and moved proximally up the tibia and distally down the metatarsal. While this is only one instance, it still indicates that the convexity of curvilinear fractures may not indicate the progressive destruction of the bone. Curvilinear fractures, their cause, and what they tell examiners about how the bone burned all need to be explored through further research to ensure that they are properly understood and that the information gained from them is accurate.

Future Avenues for Exploration

Whether or not curvilinear fractures are caused by the kinetic energy generated by muscles shrinking and pulling on the periosteum, fracturing the brittle bone underneath as the literature suggests is still unclear (Pope, 2007; Symes et al., 2008; Williams, 2020). In this study five out of the 18 curvilinear fractures observed were not located at sites of muscle attachment (May, 1970). The muscles that attach at the sites of the 13 remaining curvilinear fractures are a mix of muscles that extend and flex the limbs (May 1970). For the kinetic energy generated by a shrinking muscle to be enough to fracture bone, it would need to occur at or near a sight of muscle attachment, which in this study was not always the case. Curvilinear fractures primarily occur in fleshed remains, but they also occur in green bones and very rarely in dry bone (Baby, 1954; Binford, 1963; Buikstra and Swegle, 1989; Thurman and Wilmore, 1980; Goncalves et al, 2011). Goncalves and colleagues (2011) suggest that collagen content in the bone prior to burning may be a better indicator of why curvilinear fractures appear, but Vassalo and colleagues (2016) argue that time and temperature may be better indicators.

Further explorations of how curvilinear fractures are created and what, if anything, they can tell an examiner about the burning of the remains is needed. While observations about curvilinear fracture convexity and body position in this study seem to suggest that convexity may not point in the direction of the heat source, the sample size is too small to

be statistically significant. An *A posteriori* power analysis was conducted and the sample size needed to have the highest statistical power and effect size was 32 (Table 4.7). If a statistically significant sample size with high effect size and statistical power is used, then the relationship between fracture convexity and body position relative to the origin of a fire may be assessed with the least chance of committing a statistical type II error.

There are many other avenues to explore the questions about curvilinear fractures that still remain. A study similar to the historical studies could be conducted by burning fleshed, green, and dry bone (Baby, 1954; Binford, 1963; Buikstra and Swegle, 1989; Thurman and Wilmore, 1980; Goncalves et al., 2011). While this type of study has been done many times throughout the history of burn studies, a statistically validated relationship between the preburned state of remains and the presence of curvilinear fractures is still unclear. Questions on what causes curvilinear fractures can be better explored with a better understanding of the frequency in which they occur in bones that have no muscles and tendons. If they frequently occur in green bone, then the sole cause for their creation cannot be kinetic energy.

Another avenue to explore is if varying body positions influence the creation of curvilinear fractures. How would placing the body in a way that changes the known pattern of tissue destruction impact the formation of curvilinear fractures? If the body is positioned on its stomach, how would that impact the way the muscles burn and pull on the bone, and how then would that impact the creation of curvilinear fractures. Pope (2007) suggested that disarticulation, trauma, or dismemberment would impact the creation of curvilinear fractures. Studies could be conducted to explore if and how damaging the muscles and tendons that originate and insert into the bones impacts the prevalence and orientation of curvilinear fractures after burning. The answers to the many questions surrounding curvilinear fractures cannot be found in the current literature and will remain unanswered until more studies are conducted.

Conclusion

It is a common misconception that burning human remains destroys a body completely, like what is seen in commercial cremations. While a fire cannot destroy remains completely, it does do a large amount of damage that has an impact on how much information can be gained from remains. How burning affects remains, and the methods used to gain information from them has been extensively studied throughout the history of the field, both in an archaeological context and in a forensic one. Though like many things, despite being extensively studied, there are still many unanswered questions and ideas that need validation. One of those questions is how does curvilinear fracture convexity relates to body position relative to a fire's origin and tissue shrinkage.

This study is not able to answer the question due to small sample size but serves as a preliminary analysis of these relationship and provides a starting point for future exploration of the topic. Based on observations in this preliminary study, it appears that curvilinear fractures may indicate how heat moves along a bone but may not be related to a body's position relative to a heat source. Because of the small sample size, only a qualitative analysis could be performed, but a study with a larger sample size can be used to corroborate the observations made in this study. There is still a large dearth of information surrounding the formation of curvilinear fractures and what information, if any, they can lend to the analysis of burned remains.

LIST OF REFERENCES

Agnew AM, Bolte JH. 2012. Bone fracture biomechanics and risk. In: Crowder C, Stout SD, Editors. Bone Histology: An anthropological perspective. Boca Raton: CRC Press. p 221-240.

Baby RS. 1954. Hopewell cremation practices. In: Papers in archaeology, vol 1. Ohio Historical Society, Columbus, pp 1-7.

Binford LR. 1963. An analysis of cremations from three Michigan sites. Wisconsin Archaeology 44:98-110.

Bertocci G, Thompson A, Pierce MC. 2017. Femur fracture biomechanics and morphology associated with torsional and bending loading conditions in an in vitro immature porcine model. Journal of forensic and Legal Medicine 52:5-11.

Bohnert M, Rost T, Pollak S. 1998. The degree if destruction of human bodies in relation to the duration of the fire. Forensic Science International 95: 11-21.

Bonucci E, Graziani G. 1975. Comparative thermogravimetric, x-ray diffraction and electron microscope investigations of burnt bone from recent, ancient and prehistoric age. Accademia Nazionale dei Lincei Series 8; 59(5): 517-532.

Borrini M, Mariani PP, Murgia C, Rodriguez C, Tumbarello MV. 2012. Contextual taphonomy: superficial bone alterations as contextual indicators. Journal of Biological Research 1(LXXXV): 217-219.

Buikstra J, Goldstein L. 1973. The Perrins Ledge Crematory Illinois State Museum Report of Investigations No. 28. Illinois Valley Archaeological Program Research Papers Vol 8. Springfield, IL.

Buikstra J, Swegle M. 1989. Bone modification due to burning; experimental evidence. IN: Bone Modification. Eds. Bonnischen RB, Sorg MH. Center for the Study of the First Americans. Orono, MN. 258-278.

Cain CR. 2005. Using burned animal bone to look at Middle Stone Age occupation and behavior. Journal of Archaeological Science 32: 873-884.

Clavert P, Kempf F, Bonnomet F, Boutemy P, Marcelin L, Kahn JL. 2001. Effects of freezing/thawing on the biomechanical properties of human tendons.

Carroll El, Smith M. 2018. Burning questions: investigations using field experimentation of different patterns of change to bone in accidental vs deliberate burning scenarios. J Archaeology Science Reports 20:952-963.

Cohen J. 1992. Statistical power analysis. Current Directions in Psychological Sciences 1(3):98-101.

Costamagno S, Soulier MC, Val A, Chong S. 2019. The reference collection of cutmarks. Palethnologie 10. DOI: https://doi.org/10.4000/palethnologie.4089.

Davison KS, Siminoski K, Adachi JD, Hanley DA, Goltzman D, Hodsman AB, and colleagues. 2006. Bone strength: the whole is greater than the sum of its parts. Semin Arthristis Rhem 36:22-31.

Dempsey N, Gilbert FM, Miszkiewicz J, Oxenham MF. 2018. Biomechanical analysis of controlled tibial blunt force trauma. Australian Journal of Forensic Sciences.

Eckert WG, James S, Katchis S. 1998. Investigations of cremations and severely burned bodies. Am J Forensic Med and Path 9(3):188-200.

Ellingham STD, Thompson TJU, Islam M, Taylor G. 2015. Estimating temperature exposure of burnt bone- a methodological review. Science and Justice 55: 181-188.

Ellingham S, Sandholzer MA. 2020. Determining volumetric shrinkage trends of burnt bone using Micro-CT. Journal of Forensic Sciences 65(1):196-199.

Fernandez Castillo F, Ubelaker DH, Acosta JAL, Rossa RJE, Garcia I. 2013. The effect of temperature on bone tissue: histological change. Journal of Forensic Sciences 58(3): 578-582.

Goncalves D, Thompson TJU, Cunha E. 2011. Implications of heat-induced changes in bone on the interpretation of funerary behavior and practice. Journal of Archaeological Science 38: 1308-1313.

Gonclaves D, Cunha E, Thompson TJU. 2013. Weight references for burned human skeletal remains from Portuguese samples. Journal of Forensic Sciences 58(5): 1134-1140.

Gonclaves D, Cunha E, Thompson TJU. 2015. Estimation of the pre-burning condition of human remains in forensic contexts, International Journal of Legal Medicine 129:1137-1143.

Herrmann NP, Bennett JL. 1999. The differentiation of traumatic and heat-related fractures in burned bone. Journal of Archaeological Science 26:1-8.

Hillier ML, Bell LS. 2007. Differentiating human bone from animal bone: a review of histological methods. Journal of Forensic Sciences 52: 249-263.

Jung HJ, Vangipuram G, Fisher MB, Yang G, Hsu S, Bianchi J, Ronholdt C, Woo SLY. 2011. The effects of multiple freeze-thaw cycles on the biomechanical properties of the human bone-patella tendon-bone allograft. Journal of Orthopedic Research 1193-1198.

Klop AC, Vester MEM, Colman KL, Ruijter JA, Van Rijn RR, Oostra RJ. 2017. The effect of repeated freeze-thaw cycles on human muscle tissue visualized by postmortem computed tomography. Clinical Anatomy 30:799-804.

Krogman WM. 1943. Role of the physical anthropologist in the identification of human skeletal remains, Part 1. FBI Law Enforcement Bulletin. 12(4):17-40.

Latham KE, Madonna ME. 2007. DNA survivability in skeletal remains. In: Pokines JT, Symes SA (Eds). Manual of Forensic Taphonomy. CRC Press. Boca Raton, FL, pp. 403-425.

Lemmers SAM, Goncalves D, Cunha E, Vassalo AR, Appleby J. 2020. Burned fleshed or dry? The potential of bioerosion to determine the pre-burning condition of human remains. Journal of Archaeological Method and Theory 27(4): 972-991.

Macoveciuc I, Marques-Grant N, Horsfall I, Zioupos P. 2017. Sharp and blunt force trauma concealment by thermal alteration in homicides: an in-vitro experiment for methodology and protocol development in forensic anthropological analysis of burnt bones. Forensic Science International 275:260-271.

Mamede AP, Goncalves D, Marques MPM, Batista de Carvalho LAE. 2018. Burned bones tell their own stories: a review of methodological approaches to assess heat-induced diagenesis. Applied Spectroscopy Reviews 53(8): 603-635.

May NDS. 1970. The anatomy of the sheep; a dissection manual. 3rd edition. Australia University of Queensland Press. St. Lucia.

McCutcheon P. 1992. Burned archaeological bone. IN: Deciphering a Shell Midden. Eds. Stein JK. Academic Press. San Diego, CA.

Marcniak SM. 2019. A preliminary assessment of the identification of saw marks on burned bone. Journal of Forensic Sciences 54(4): 779-785.

MiKinley JI. 2006. Cremation… the cheap option? In: Kunusel C, Gowland R (Eds.), The Social Archaeology of Human Remains. Oxbow Books, Oxford; 81-88.

Pasquini C, Spurgeon TL, Pasquini S, Smith M. 1995. Anatomy of domestic animals: systemic and regional approach. 7 ed. Sudz Publishing, Pilot Point, TX.

Pokines JT, King RE, Graham DD, Costello AK, Adams DM, Pendray JM, Rao Kushal, Siwek. 2016. The effects of experimental freeze-thaw cycles to bone as a component of subaerial weathering. J Arch Sci 6: 594-602.

Pope EJ. 2007. The effect of fire on human remains: characteristics of taphonomy and trauma. (UMI Number: 3292654) [Doctoral dissertation, University of Arkansas] ProQuest Dissertations Publishing.

Pope EJ, Smith OC. 2004. Identification of traumatic injury in burned cranial bones: an experimental approach. Journal of Forensic Sciences 49(3): 431-440.

Ren D, Sun K, Tian S, Yang X, Zhang C, Wang W, Huang H, Zhang J, Deng Y. 2012. Effects of gamma irradiation and repetitive freeze-thaw cycles on the biomechanical properties of human flexor digitorum superficialis tendons. Journal of Biomechanics 45:252-256.

Reidsma FH, van Hoesel A, van Os BJH, Megens L, Braadbaart F. 2016. Charred bone: physical and chemical changes during laboratory simulated heating under reducing conditions and its relevance for the study of fire in archaeology. Journal of Archaeological Science 10: 282-292.

Rossi D, Gruchy DE, Lovell NC. 2004. A comparative experiment in the consolidation of cremated bone. International Journal of Osteoarcheology 14:104-111.

Shipman P, Foster G, Schoeninger M. 1984. Burnt bones and teeth: an experimental study of color, morphology, crystal structure and shrinkage. Journal of Archaeological Sciences 11:307-325.

Siegert CC, Hamilton MD, Erhart E, Devline J. 2018. The application of consolidation materials to burned bone: a comparative approach. AAFS Proceedings 2018.

Symes SA, Rainwater CW, Chapman EN, Gipson DR, Piper Al. 2008. Patterned thermal destruction in a forensic setting. IN: Schmidt CW and Symes SA (Eds.). The analysis of burned human remains. Academic Press. San Diego, CA, pp. 17-59.

Symes SA, L'Abbe EN, Pokines JT, Yuzwa T, Messer D, Stormquist A, Keough N. 2014. Thermal alterations to bone. IN: Pokines JT and Symes SA (Eds.). Manual of Forensic Taphonomy. CRC Press. Boca Raton, FL, pp. 367-407.

Thompson TJU. 2004. Recent advances in the study of burned bone and their implications for forensic anthropology. Forensic Science International 146S: S203-S205.

Thompson TJU. 2005. Heat-induced dimensional changes in bone and their consequences for forensic anthropology. Journal of Forensic Sciences 50(5): 1-8.

Thompson TJU, Chudek JA. 2007. A novel approach to the visualization of heat-induced structural change in bone. Science and Justice 47:99-104.

Thompson TJU, Islam M, Piduru K, Marcel A. 2011. An investigation into the internal and external variables acting on crystallinity index using Fourier Transform Infrared Spectroscopy on unaltered and burned bone. Paleogeography, paleoclimatology, Paleoecology 299:168-174.

Thurman MD, Willmore LJ. 1980. A replicative cremation experiment. North American Archaeologist 2(4): 275-283.

Topoleski JJ, Christensen AM. 2019. The use of a gelatin-based consolidant to preserve thermally altered remains. American Academy of Forensic Science. Baltimore, MD.

Trotter M, Peterson RR. 1955. Ash weight of human skeletons in per cent of their dry, fat-free weight. Anatomical Record 123(3):341-358.

Ubelaker DH. 2009. The forensic evaluation of burned skeletal remains: a synthesis. Forensic Science International 183: 1-5.

Vassalo AR, Cunha E, Batista de Carvalho LAE, Goncalves D. 2016. Rather yield than break: assessing the influence of human bone collagen content on heat-induced warping through vibrational spectroscopy. International Journal of Legal Medicine 130:1647-1656.

Warren MW, Schultz JJ. 2002. Post-cremation taphonomy and artifact preservation, Journal of Forensic Sciences 47(3): 656-659.

Waterhouse K. 2013. The effect of victim age on burnt bone fragmentation: implications for remains recovery. Forensic Science International 231: 409.e1-409.e7.

Webb WS, Snow CE. 1945. The Adena people. Reports in Archaeology and Anthropology VI. University of Kentucky, Lexington.

Williams AN. 2020. A new classification system for analyzing burned human remains. (ProQuest Number: 27998511) [Doctoral dissertation, University of Montana] ProQuest Dissertations Publishing.

Zana M, Magli F, Mazzucchi A, Castoldi E, Gibelli D, Caccia G, Cornacchia F, Gaudio DA, Mattia M, Cattaneo C. 2017. Effects of cremation on fetal bones. Journal of Forensic Sciences 62(5): 1140-1144.

APPENDIX

Appendix A: Data collection forms for all burns.

Table 3.2. Data collection forms for all burns.

Specimen number: 2020-1 Fore
Observer Name: K.Cheek Date: 1/30/20 Time started: 10:00am Time stopped:11:20am

Time:	Temperature (F)	Ambient Temperature	Approximate % of muscle remaining	Muscle shrinkage observations	Fire progression observations
0 min	37	34	100%	N/A	0%
20 min	536+	37	100%	Both limbs are curling	50%
40 min	536+	34	95%	Both limbs curled in completely, right limb has fractured, and bone is exposed on both	50%
60 min	536+	36	80%	R limb mostly calcined l limb partially calcined	100%
80 min	536+	37	75%	Tissue burning on shoulders and observable shrinkage	100%

Specimen number: 2020-1 Hind
Observer Name: K. Cheek Date: 1/26/20 Time started: 11:40 Time stopped: 4:20

Time:	Temperature (F)	Ambient Temperature	Approximate % of muscle remaining	Muscle shrinkage observations	Fire progression observations
0 min	62	52	100%	N/A	0%
20 min	536+	59	100%	N/A	50%
40 min	536+	61	100%	Left hoof points slightly and limb extends	50%
60 min	536+	62	100%	Both slightly extend	50%
80 min	536+	62	95%	Left limb posterior muscles burned and the lumbar verts	100%
100 min	536+	62	95%	Left limb broken and fell right limb extends	100%
120 min	536+	65	95%	No change	100%

Table 3.2. Continued

Time:	Temperature (F)	Ambient Temperature	Approximate % of muscle remaining	Muscle shrinkage observations	Fire progression observations
140 min	536+	62	90%	No change	100%
160 min	536+	63	85%	Muscles of the hind are burning	100%
180 min	536+	61	75%	Right limb starts to burn posteriorly	100%
200 min	536+	62	65%	Most of proximal right limb is consumed	100%

Specimen number: 2020-2 Fore
Observer Name: K. Cheek Date: 1/26/20 Time started: 11:40 Time stopped: 4:20

Time:	Temperature (F)	Ambient Temperature	Approximate % of muscle remaining	Muscle shrinkage observations	Fire progression observations
0 min	100	40	100%	N/A	0%
20 min	536+	37	97%	R limb has curled up and in bone is exposed at the elbow joint left limb not as burned	65%
40 min	536+	38	80%	L limb started to curl towards stomach posteriorly exposed bone around elbow. Right limb shoulder muscles contract	70%
60 min	536+	35	70%	No change	100%
80 min	536+	36	60%	Majority of tissue charred.	100%

Specimen number: 2020-2 Hind
Observer Name: K. Cheek Date: 2/6/20 Time started: 9:30 Time stopped: 12:10

Time:	Temperature (F)	Ambient Temperature	Approximate % of muscle remaining	Muscle shrinkage observations	Fire progression observations
0 min	34	26	100%	N/A	0%
20 min	536+	26	100%	N/A	25%
40 min	536+	32	100%	N/A	30%

Table 3.2. Continued

Time:	Temperature (F)	Ambient Temperature	Approximate % of muscle remaining	Muscle shrinkage observations	Fire progression observations
60 min	536+	32	100%	Left leg curls up and rump is burning	50%
80 min	536+	22	90%	L leg curled all the way in with calcination r leg not moved much. L leg about to fall	66%
100 min	536+	33	80%	L leg broken and fallen no change to femur right leg started to curl	100%
120 min	536+	32	75%	Muscles in upper part of r limb is burning up lower not burning	100%
140 min	536+	33	65%	Muscles gone from posterior no major shrinkage	100%
160 min	536+	36	60%	R limb falls	100%

Specimen number: 2020-3 Fore
Observer Name: K. Cheek Date: 1/29/20 Time started: 9:22 Time stopped: 12:03

Time:	Temperature (F)	Ambient Temperature	Approximate % of muscle remaining	Muscle shrinkage observations	Fire progression observations
0 min	32	36	100%	N/A	0%
20 min	207	36	100%	N/A	25%
40 min	536+	30	100%	Left limb curls in	30%
60 min	536+	32	100%	Both curl in	50%
80 min	536+	34	95%	Hooves to shoulder no exposed bone	60%
100 min	536+	32	90%	Bone exposed on the right limb	100%
120 min	536+	34	85%	More flesh on the right consumed	100%
140 min	536+	36	80%	Bone exposed on both limbs	100%

Table 3.2. Continued

Time:	Temperature (F)	Ambient Temperature	Approximate % of muscle remaining	Muscle shrinkage observations	Fire progression observations
160 min	536+	34	70%	N/A	100%

Specimen number: 2020-3 Hind
Observer Name: K. Cheek Date: 1/29/20 Time started: 12:55 Time stopped: 3:55

Time:	Temperature (F)	Ambient Temperature	Approximate % of muscle remaining	Muscle shrinkage observations	Fire progression observations
0 min	50	36	100%	N/A	0%
20 min	536+	34	97%	Distal limbs very burnt	50%
40 min	536+	39	95%	Left limb broke right limb calcined	100%
60 min	536+	39	95%	N/A	100%
80 min	536+	39	90%	Both legs broken and fell flank starting to contract	100%
100 min	536+	39	85%	Left knee exposed	100%
120 min	536+	39	75%	N/A	100%
140 min	536+	37	70%	N/A	100%
160 min	536+	32	65%	N/A	100%
180 min	536+	37	60%	N/A	100%

Specimen number: 2020-4 Fore
Observer Name: K. Cheek Date: 1/28/20 Time started: 1:45 Time stopped: 4:45

Time:	Temperature (F)	Ambient Temperature	Approximate % of muscle remaining	Muscle shrinkage observations	Fire progression observations
0 min	48	36	100%	N/A	0%
20 min	536+	36	97%	Left limb contracts	50%
40 min	536+	32	85%	Both curl in	100%
60 min	536+	32	80%	Right limb breaks	100%
80 min	536+	36	75%	Slight shoulder contraction	100%
100 min	536+	40	65%	Same	100%
120 min	536+	40	55%	Same	100%

Table 3.2. Continued
Specimen number: 2020-4 Hind
Observer Name: K. Cheek Date: 1/28/20 Time started: 9:40 Time stopped: 1:00

Time:	Temperature (F)	Ambient Temperature	Approximate % of muscle remaining	Muscle shrinkage observations	Fire progression observations
0 min	33	33	100%	N/A	0%
20 min	53	33	100%	N/A	30%
40 min	53	33	100%	N/A	50%
60 min	56	34	100%	N/A	50%
80 min	170	36	100%	Both limbs extend	60%
100 min	470	32	95%	L hind posterior muscles exposed and rump burning	100%
120 min	536+	37	90%	L limb broke and most muscle is gone right post muscles burning	100%
140 min	536+	33	85%	Both shift laterally	100%
160 min	536+	35	80%	Left is calcined right posterior is burning	100%
180 min	536+	35	80%	Right slowly burning	100%
200 min	536+	35	70%	Muscles around tibia gone	100%

Appendix B: Uniformity Scores.

Table 4.1. Uniformity scores organized by element and side. Score move from the proximal ¼ to the distal ¼ of each element.

Uniformity Score Proximal to Distal						
Specimen/Limb pair	Side	Element	1st 1/4	2nd 1/4	3rd 1/4	4th 1/4
2020-1 Hind	Left	Femur	4	1	1	2
2020-1 Hind	Right	Femur	2	1	1	2
2020-2 Hind	Left	Femur	1	1	1	3
2020-2 Hind	Right	Femur	2	1	1	5
2020-3 Hind	Left	Femur	1	1	1	4
2020-3 Hind	Right	Femur	1	1	1	2
2020-4 Hind	Left	Femur	1	1	2	3
2020-4 Hind	Right	Femur	1	1	1	1
2020-1 Fore	Left	Humerus	3	2	1	2
2020-1 Fore	Right	Humerus	2	1	1	1
2020-2 Fore	Left	Humerus	3	2	2	2
2020-3 Fore	Left	Humerus	2	1	1	1
2020-3 Fore	Right	Humerus	2	1	1	2
2020-4 Fore	Left	Humerus	1	1	1	1
2020-4 Fore	Right	Humerus	1	1	1	2
2020-2 Fore	Right	Humerus	5	3	3	2
2020-1 Fore	Right	Metacarpal	1	1	1	1
2020-3 Fore	Left	Metacarpal	2	n/a	1	2
2020-1 Fore	Left	Metacarpal	2	2	2	1
2020-2 Fore	Left	Metacarpal	4	4	3	1
2020-2 Fore	Right	Metacarpal	4	4	4	3
2020-3 Fore	Right	Metacarpal	2	4	4	3
2020-4 Fore	Left	Metacarpal	3	3	3	3
2020-4 Fore	Right	Metacarpal	3	3	4	3
2020-1 Hind	Right	Metatarsal	1	1	1	1
2020-2 Hind	Right	Metatarsal	2	2	2	1
2020-4 Hind	Right	Metatarsal	1	1	1	1
2020-1 Hind	Left	Metatarsal	2	2	4	4
2020-3 Hind	Right	Metatarsal	2	2	2	3
2020-2 Hind	Left	Metatarsal	3	2	3	4
2020-3 Hind	Left	Metatarsal	2	3	2	3
2020-4 Hind	Left	Metatarsal	3	2	4	2
2020-1 Fore	Left	Radius	3	4	3	3
2020-1 Fore	Right	Radius	2	4	3	3
2020-2 Fore	Left	Radius	5	4	3	5
2020-2 Fore	Right	Radius	5	3	3	4
2020-3 Fore	Left	Radius	1	1	3	3
2020-3 Fore	Right	Radius	3	2	2	3
2020-4 Fore	Left	Radius	1	3	2	5
2020-4 Fore	Right	Radius	2	3	4	3
2020-1 Hind	Left	Tibia	1	2	3	2
2020-1 Hind	Right	Tibia	2	2	2	1
2020-2 Hind	Left	Tibia	2	2	4	5
2020-2 Hind	Right	Tibia	2	3	3	5
2020-4 Hind	Left	Tibia	2	3	4	3
2020-4 Hind	Right	Tibia	1	1	2	3
2020-3 Hind	Left	Tibia	4	4	5	5
2020-3 Hind	Right	Tibia	2	3	3	4
2020-1 Fore	Left	Ulna	1	2	2	2
2020-1 Fore	Right	Ulna	n/a	2	1	n/a
2020-2 Fore	Left	Ulna	2	4	2	1
2020-2 Fore	Right	Ulna	3	n/a	4	3
2020-3 Fore	Left	Ulna	1	1	1	n/a
2020-3 Fore	Right	Ulna	3	3	n/a	n/a
2020-4 Fore	Left	Ulna	1	2	n/a	n/a
2020-4 Fore	Right	Ulna	4	2	n/a	n/a

Appendix C: Color Scores.

Table 4.2. Color scores organized by element and side. Score move from the proximal ¼ to the distal ¼ of each element.

			Color Score Proximal to Distal			
Specimen/Limb pair	Side	Element	1st 1/4	2nd 1/4	3rd 1/4	4th 1/4
2020-1 Hind	Left	Femur	1	1	1	1
2020-1 Hind	Right	Femur	1	1	1	1
2020-2 Hind	Left	Femur	1	1	1	1
2020-2 Hind	Right	Femur	1	1	1	3
2020-3 Hind	Left	Femur	1	1	1	4
2020-3 Hind	Right	Femur	1	1	1	1
2020-4 Hind	Left	Femur	1	1	1	3
2020-4 Hind	Right	Femur	1	1	1	1
2020-1 Fore	Left	Humerus	1	1	1	1
2020-1 Fore	Right	Humerus	1	1	1	1
2020-2 Fore	Left	Humerus	1	1	1	1
2020-3 Fore	Left	Humerus	1	1	1	1
2020-3 Fore	Right	Humerus	1	1	1	1
2020-4 Fore	Left	Humerus	1	1	1	1
2020-4 Fore	Right	Humerus	1	1	1	1
2020-2 Fore	Right	Humerus	4	3	3	3
2020-1 Fore	Right	Metacarpal	1	1	1	1
2020-3 Fore	Left	Metacarpal	1	n/a	1	1
2020-1 Fore	Left	Metacarpal	3	3	3	1
2020-2 Fore	Left	Metacarpal	3	3	1	1
2020-2 Fore	Right	Metacarpal	3	5	3	3
2020-3 Fore	Right	Metacarpal	3	5	4	3
2020-4 Fore	Left	Metacarpal	3	3	3	1
2020-4 Fore	Right	Metacarpal	4	4	3	1
2020-1 Hind	Right	Metatarsal	1	1	1	1
2020-2 Hind	Right	Metatarsal	1	1	1	1
2020-4 Hind	Right	Metatarsal	1	1	1	1
2020-1 Hind	Left	Metatarsal	3	3	4	4
2020-3 Hind	Right	Metatarsal	3	3	3	3
2020-2 Hind	Left	Metatarsal	4	5	5	6
2020-3 Hind	Left	Metatarsal	5	5	3	3
2020-4 Hind	Left	Metatarsal	6	5	5	1
2020-1 Fore	Left	Radius	1	3	4	6
2020-1 Fore	Right	Radius	3	4	5	6
2020-2 Fore	Left	Radius	4	5	6	5
2020-2 Fore	Right	Radius	4	5	5	5
2020-3 Fore	Left	Radius	1	1	3	3
2020-3 Fore	Right	Radius	3	4	5	6
2020-4 Fore	Left	Radius	1	3	3	3
2020-4 Fore	Right	Radius	3	4	4	5
2020-1 Hind	Left	Tibia	1	3	3	3
2020-1 Hind	Right	Tibia	1	1	1	1
2020-2 Hind	Left	Tibia	1	1	3	4
2020-2 Hind	Right	Tibia	1	1	3	3
2020-4 Hind	Left	Tibia	1	3	3	6
2020-4 Hind	Right	Tibia	1	1	1	3
2020-3 Hind	Left	Tibia	3	4	4	5

Table 4.2 continued.

Specimen/Limb pair	Side	Element	1st 1/4	2nd 1/4	3rd 1/4	4th 1/4
2020-3 Hind	Right	Tibia	3	3	3	4
2020-1 Fore	Left	Ulna	1	3	4	5
2020-1 Fore	Right	Ulna	n/a	4	4	n/a
2020-2 Fore	Left	Ulna	1	4	6	6
2020-2 Fore	Right	Ulna	1	n/a	6	6
2020-3 Fore	Left	Ulna	1	1	1	n/a
2020-3 Fore	Right	Ulna	3	5	n/a	n/a
2020-4 Fore	Left	Ulna	1	1	n/a	n/a
2020-4 Fore	Right	Ulna	3	3	n/a	n/a

Appendix D: Curvilinear presence and absence, convexity, and location.

Table 4.3. Scoring of curvilinear fracture presence and absence, if convexity is in the anticipated direction, and location of the fracture(s) on the bone.

Specimen/Limb pair	Side/Element	Curvilinear Fracture	Convex Distally	Location on bone
2020-1 Fore	Right Humerus	0	n/a	
	Right Ulna	0	n/a	
	Right Radius	1	1	Posterior Proximal Shaft
	Right Metacarpal	0	n/a	
	Left Humerus	0	n/a	
	Left Ulna	1	1	Posterior Midshaft
	Left Radius	1	1	Posterior Midshaft
	Left Metacarpal	0	n/a	
2020-1 Hind	Right Femur	0	n/a	
	Right Tibia	0	n/a	
	Right Metatarsal	0	n/a	
	Left Femur	0	n/a	
	Left Tibia	0	n/a	
	Left Metatarsal	0	n/a	
2020-2 Fore	Right Humerus	0	n/a	
	Right Ulna	0	n/a	
	Right Radius	1	1	Posterior Midshaft
	Right Metacarpal	1	0	Posterior Distal Shaft
	Left Humerus	0	n/a	
	Left Ulna	1	1	Medial Midshaft
	Left Radius	1	1	Posterior Proximal Midshaft
	Left Metacarpal	0	n/a	
2020-2 Hind	Right Femur	0	n/a	
	Right Tibia	1	1	Lateral Midshaft
	Right Metatarsal	0	n/a	
	Left Femur	0	n/a	
	Left Tibia	1	1	Posterior Lateral Midshaft
	Left Metatarsal	0	n/a	

Table 4.3 continued.

Specimen/Limb pair	Side/Element	Curvilinear Fracture	Convex Distally	Location on bone
2020-3 Fore	Right Humerus	0	n/a	
	Right Ulna	0	n/a	
	Right Radius	1	1	Posterior Proximal Shaft
	Right Metacarpal	0	n/a	
	Left Humerus	0	n/a	
	Left Ulna	0	n/a	
	Left Radius	0	n/a	
	Left Metacarpal	0	n/a	
2020-3 Hind	Right Femur	0	n/a	
	Right Tibia	0	n/a	
	Right Metatarsal	0	n/a	
	Left Femur	0	n/a	
	Left Tibia	1	1	Posterior Midshaft
	Left Metatarsal	0	n/a	
2020-4 Fore	Right Humerus	0	n/a	
	Right Ulna	1	0	Medial Proximal End
	Right Radius	1	1	Posterior Proximal Shaft
	Right Metacarpal	1	0	Posterior Distal Shaft
	Left Humerus	0	n/a	
	Left Ulna	0	n/a	
	Left Radius	0	n/a	
	Left Metacarpal	1	0	Medial Distal Shaft
2020-4 Hind	Right Femur	0	n/a	
	Right Tibia	0	n/a	
	Right Metatarsal	0	n/a	
	Left Femur	0	n/a	
	Left Tibia	1	1	Posterior Lateral and Anterior Midshaft
	Left Metatarsal	1	1	Medial Proximal End

VITA

Kimber Cheek was born and raised in Fredericksburg, VA. In high school she developed a love for forensic science and after taking anatomy, was led to pursue an anthropology degree. She received her BA in anthropology from Radford University in May of 2018 with minors in biology and forensic science. Her time at Radford was filled with amazing mentors in the Anthropological Sciences department, the Honors Academy, and through her internship with the FBI, which led to her eventual acceptance into the Anthropology MA program at the University of Tennessee, Knoxville. Since coming to UTK, she has had many great experiences and learned many things. Her thesis took longer than planned due to the COVID-19 pandemic and beginning a full-time job to pay for her extended time in the program. Once her thesis is completed, she plans to take some time to work and be a "real person" for a little while as she likes to tell her friends. Eventually, she will reevaluate whether she wants to return to academia or take the skills and knowledge she has gained from her degrees and apply them to a job outside of academia.